論文 / 著書情報
Article / Book Information

Title	Dynamic analysis of 3D printed lattice sandwich beam with square grid core
Authors	Yi-Chuang Wu, Yun-Jhen Lai, Jhen-Hao Syu, Ming Ji
Citation	Journal of Mechanics, Volume 41, , Page 103–128
Pub. date	2025, 3
DOI	https://doi.org/10.1093/jom/ufaf009
Copyright	Information is in the article.

Journal of Mechanics, 2025, **41**, 103–128
https://doi.org/10.1093/jom/ufaf009
Regular Article

OXFORD

Dynamic analysis of 3D printed lattice sandwich beam with square grid core

Yi-Chuang Wu [1,2,3], Yun-Jhen Lai[2], Jhen-Hao Syu[2] and Ming Ji [4,*]

[1]Department of Mechanical Engineering, National Taiwan University of Science and Technology, Taipei, Republic of China
[2]Department of Mechanical Engineering, National Chung Cheng University, Chiayi, Republic of China
[3]Advanced Institute of Manufacturing with High-tech Innovations, National Chung Cheng University, Chiayi, Republic of China
[4]Institute of Integrated Research, Institute of Science Tokyo, Yokohama, Japan

*Corresponding author: ji.m.aa@m.titech.ac.jp

ABSTRACT

In this paper, the vibration characteristics of sandwich beams with square grid cores are investigated theoretically, numerically and experimentally. The natural frequencies of the sandwich beams are calculated by Euler–Bernoulli theory and equivalent parameters. The theoretical results are validated by using numerical and experimental results. Two simulation methods: equivalent simulation and detailed simulation are used. In the equivalent simulation, the material is assumed to be isotropic with the equivalent material properties. The natural frequencies and mode shapes of 3D-printed sandwich beams are measured using the amplitude-fluctuation electronic speckle pattern interferometry. It is found that filling metal mixture into the cores only changes the equivalent density. The equivalent stiffness is almost the same. Thus, it is possible to control the vibration characteristics of sandwich beams by filling a metal mixture into the cores with almost constant stiffness. Then, the composite sandwich beams with different square grid cores are studied theoretically, numerically and experimentally. The results obtained from different methods are in good agreement with each other. The study offers a method to control the structural vibration characteristics of sandwich beams by changing the design of the square cores and filling the cores with metal mixture.

KEYWORDS: sandwich beams with square grid cores, 3D printing, composite sandwich beams, AF-ESPI

1. INTRODUCTION

The sandwich composites comprising two faces and a lightweight core, have been widely applied in numerous industries, because of high thermal insulation properties, ultra-light structural weight and high specific stiffness/strength. The vibration characteristics of the sandwich structures have gained numerous interests in recent years. However, there is limited research about experimental measurements of sandwich structures with cores. One potential reason is that it is difficult to fabricate sandwich structures with square grid cores. As the development of 3D printing technology, it offers a suitable method to fabricate sandwich structures with complicated cores.

Souza Eloy *et al.* [1] fabricated sandwich beams with honeycomb cores using a 3D printer. The dynamic properties of sandwich beams with honeycomb cores filled with a magnetorheological elastomer (MRE) were investigated numerically and experimentally. The vibration characteristics of the structures can be controlled by increasing an induced magnetic field. Faria *et al.* [2] experimentally investigated the free and forced vibrations of sandwich beams with two types of cores: square and hexagonal cores, filled with magnetorheological gels. Chikh *et al.* [3] investigated the active vibration control of sandwich beams with a MRE core experimentally and numerically. The equivalent method is an efficient method to investigate the vibration of sandwich structures. Gibson and Ashby [4] have given relative densities of different cellular structures and used three bending test to obtain the equivalent stiffness. Wang *et al.* [5] applied a homogenization method to evaluate the effective material properties of the hierarchical composite square-honeycomb cores, and predicted the natural frequencies using the equivalent model. Gu *et al.* [6] proposed an equivalent method to predict the natural frequencies of a square grid sandwich plate. They discussed the influences of material parameters and geometric sizes on the equivalent thickness, density and Young's modulus. Steenackers *et al.* [7] did the finite element analysis of sandwich structures with honeycomb cores using the equivalent models. It proved that an appropriate equivalent model can reduce the computation time of finite element models. Wang and McDowell [8] discussed the in-plane mechanical properties of 7 types of periodic honeycomb structures. And they gave the relationships between effective elastic stiffness and relative density of periodic honeycomb structures. Lu *et al.* [9] used finite element analysis and three-point bending test to characterize the equivalent mechanical properties of 3D printed sandwich composites with Bi-Grid, Tri-Grid, Quadri-Grid and Kagome-Grid honeycomb cores. Yao *et al.* [10] investigated the ultimate tensile strength of 3D printed polylactic acid materials with different printing angles theoretically and experimentally.

Received: 9 December 2024; **Revised:** 12 February 2025; **Accepted:** 17 March 2025

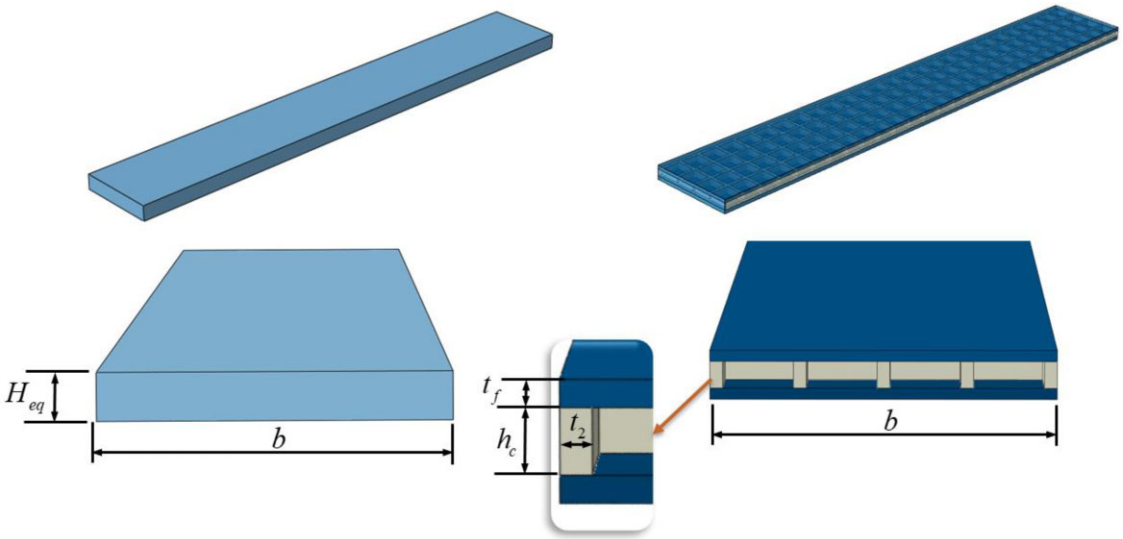

Figure 1 Schematic of a sandwich beam with square grid core.

Fernandez-Vicente *et al.* [11] studied the influences of pattern and density of the infill on the tensile strength of printed specimens. It proved that the combination of a rectilinear pattern in a 100% infill has higher tensile strength. Dai and Zhang [12] applied the energy equivalence method to study the size effects of the periodic core cells of free vibration analysis.

There are a few papers about the experimental measurements of the dynamic properties of the sandwich structures with cores, especially the mode shapes. The amplitude-fluctuation electronic speckle pattern interferometry (AF-ESPI) is a full-field, non-contact technique for measuring the displacement of a vibrating surface. The prior research was conducted by Butters and Leendertz [13], Høgmoen and Løkberg [14] and Moore and Tyrer [15]. Then, Wang *et al.* [16] applied time-averaged electronic speckle pattern interferometry methods to measure the vibration of composite plates. Ma and his collaborators developed the AF-ESPI to measure the vibration of isotropic plates [17–20], isotropic plates coupled with fluid [21–24], laminated composite plates [25], piezoceramic plates [26–35] and piezoelectric shells [36, 37]. Ji *et al.* [38] applied the Gormon superposition method to investigate the dynamic characteristics of thin rectangular plates with multiple bolts and stand-off supports, and used AF-ESPI to validate the proposed theory. Wu and his collaborators [39, 40] applied the AF-ESPI to investigate the design of efficient surface electrodes of piezoceramic plates. Then, Ji *et al.* [41] designed an annular membrane internally connected with a piezoceramic disk. And the model was validated by the natural frequencies and mode shapes measured by AF-ESPI.

To investigate the vibration characteristics of sandwich beams with square grid cores, the natural frequencies of the sandwich beams are calculated by Euler–Bernoulli theory and equivalent parameters first. The theoretical results are validated by using numerical and experimental results. Two simulation methods: equivalent simulation and detailed simulation are used. In the equivalent simulation, the material is assumed to be isotropic with the equivalent material properties. The natural frequencies and mode shapes of 3D-printed sandwich beams are measured using the AF-ESPI. It is found that filling metal mixture into the cores only changes the equivalent density. The equivalent stiffness is almost the same. Thus, it is possible to control the vibration characteristics of sandwich beams by filling a metal mixture into the cores with almost constant stiffness. Then, the composite sandwich beams with different square grid cores are studied theoretically, numerically and experimentally. The results obtained from different methods are in good agreement with each other.

2. THEORETICAL FORMULATION

A sandwich beam with a square grid core is shown in Fig. 1. The length and width of the beam are L and b, respectively. The face beams are of the same thickness t_f. The thickness of the core is h_c. The wall thickness of the square grid is t_2. The equivalent beam theory is used to conduct the dynamic analysis. The Euler–Bernoulli beam theory is expressed as

$$E_{eq}I_{eq}\frac{\partial^4 y}{\partial x^4} + \rho_{eq}A_{eq}\frac{\partial^2 y}{\partial t^2} = 0, \tag{1}$$

where E_{eq} is the equivalent Young's modulus; $I_{eq} = H_{eq}^3 b/12$ is the equivalent second moment of area; ρ_{eq} is the equivalent density; $A_{eq} = H_{eq}b$ is the equivalent area; H_{eq} is the equivalent thickness of the sandwich beam; y is the transverse displacement; x is the coordinate in the length direction; and t is time. The harmonic vibration of a cantilevered beam can be easily solved.

$$y(x,t) = [C_1(\sinh(\beta x) - \sin(\beta x)) + C_2(\cosh(\beta x) - \cos(\beta x))]\, e^{i\omega t}, \tag{2}$$

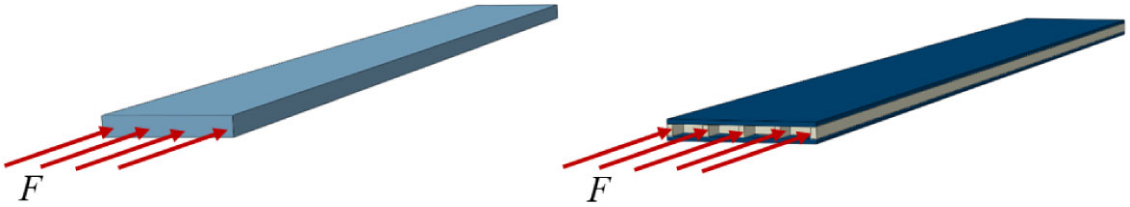

Figure 2 Schematic of an equivalent beam and a sandwich beam under compression along the length direction.

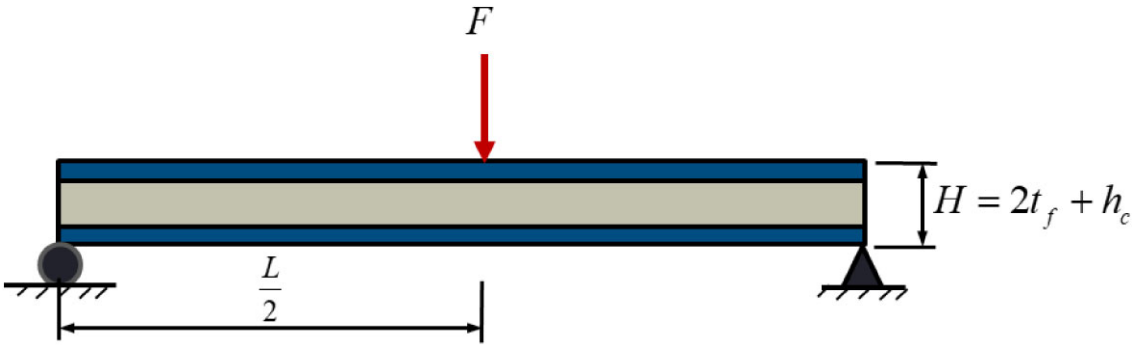

Figure 3 Schematic of three-point bending test of a sandwich beam.

where ω is the annular frequency; $\mathrm{i} = \sqrt{-1}$; $\beta^4 = \omega^2 \rho_{eq} A_{eq}/(E_{eq} I_{eq})$; C_1 and C_2 are unknown constants. The parameter β satisfies

$$\cos \beta L \cosh \beta L = -1 \tag{3}$$

Figure 2 shows the schematic of an equivalent beam and a sandwich beam under compression along the length direction. The force F can be expressed as

$$F = E_{eq} \varepsilon H_{eq} b, \tag{4}$$

where ε is strain. Taking the core in Fig. 1 as example, the cross-sectional area is $A_s = 2t_f b + 5h_c t_2$. Thus, the force can also be expressed as

$$F = E_s \varepsilon A_s = E_s \varepsilon \left(2t_f b + 5h_c t_2\right). \tag{5}$$

From Eqs. (4) and (5), the following equation can be obtained.

$$b H_{eq} E_{eq} = E_s \left(2t_f b + 5h_c t_2\right), \tag{6}$$

where E_s is the Young's modulus of the printing material. If the core has m grids, Eq. (6) becomes

$$b H_{eq} E_{eq} = E_s [2t_f b + (m+1) h_c t_2]. \tag{7}$$

Figure 3 shows three-point bending test of a sandwich beam. The maximum deflection is

$$\delta = \frac{F L^3}{48 E_{eq} I_{eq}}. \tag{8}$$

The equivalent bending stiffness of the example in Fig. 1 is

$$E_{eq} \frac{b H_{eq}^3}{12} = \frac{E_f b t_f^3}{6} + \frac{E_f b t_f}{2} (t_f + h_c)^2 + \frac{5 E_s t_2 h_c^3}{12}, \tag{9}$$

where E_f represents the Young's modulus of the face beam. For the core with m grids, the bending stiffness is

$$E_{eq} \frac{b H_{eq}^3}{12} = \frac{E_f b t_f^3}{6} + \frac{E_f b t_f}{2} \left(t_f + h_c\right)^2 + \frac{(m+1) E_s t_2 h_c^3}{12}. \tag{10}$$

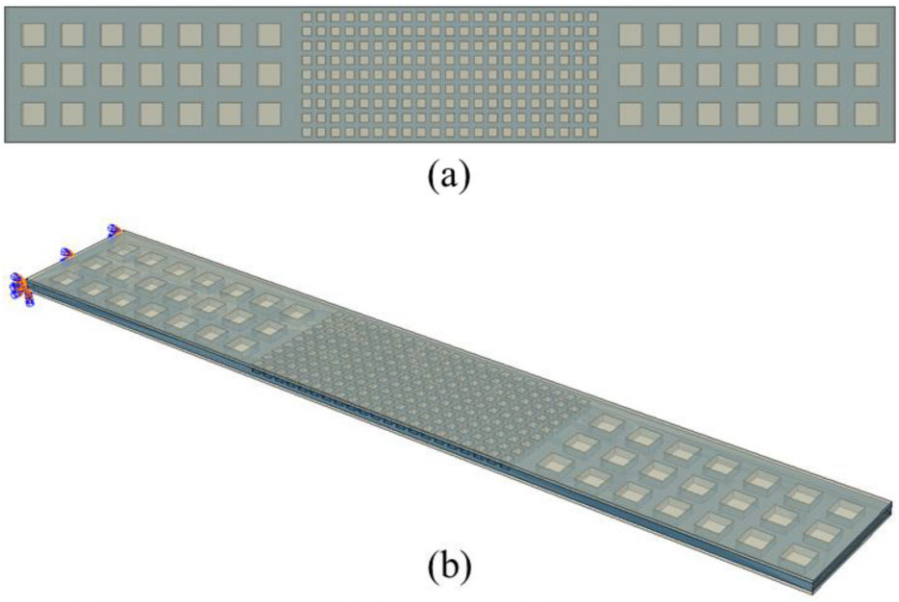

Figure 4 An example of a composite sandwich beam with three blocks square grid cores (a) Top view (b) Three view.

In this study, the materials of the face and the core are same, thus, $E_s = E_f$. From Eqs. (7) and (10), the equivalent thickness of the sandwich beam can be solved as

$$H_{eq} = \sqrt{\frac{2bt_f^3}{2t_f b + (m+1)\,t_2 h_c} + \frac{6t_f b\left(t_f + h_c\right)^2}{2t_f b + (m+1)\,t_2 h_c} + \frac{(m+1)\,t_2 h_c^3}{2t_f b + (m+1)\,t_2 h_c}}. \tag{11}$$

Then, the equivalent Young's modulus is

$$E_{eq} = \frac{E_s\left[2bt_f + (m+1)h_c t_2\right]}{bH_{eq}}. \tag{12}$$

The equivalent density of the sandwich beam is calculated by using

$$\rho_{eq} = \frac{2\rho_f\left(Lbt_f\right) + \rho_c\left[Lbh_c - (n \times m)\,s^2 h_c\right]}{LbH_{eq}}, \tag{13}$$

where ρ_f is the density of the face beam and ρ_c is the density of the core.

In this study, not only the sandwich beams with square grid core, but also the composite sandwich beams with different grid cores are investigated. Figure 4 shows an example of a composite sandwich beam with 3 blocks square grid cores. The equation of motion of each component of the sandwich beam is

$$E_k I_k \frac{\partial^4 f_k}{\partial x_k^4} + \rho_k A_k \frac{\partial^2 f_k}{\partial t^2} = 0, \tag{14}$$

where $I_k = b_k h_k^3/12$; $A_k = b_k h_k$; b_k is the width of the kth component of the composite beam; h_k is the thickness of the kth component; E_k is Young's modulus of the kth component's material; ρ_k is the density of the kth component's material; x_k is the coordinate of the kth component of the composite beam in the length direction, $0 \le x_k \le L_k$; and f_k is the transverse displacement of the kth component. For the harmonic vibration, Eq. (14) becomes

$$\frac{\partial^4 F_k}{\partial x_k^4} - \beta_k^4 F_k = 0, \tag{15}$$

where $\beta_k^4 = \rho_k A_k \omega^2/(E_k I_k)$. For convenience, the non-dimensional variables $\zeta_k = x_k/L_k, \bar{F}_k = F_k/L_k$ and $\bar{\beta}_k = \beta_k L_k$ are used. Then, Eq. (15) can be rewritten as

$$\frac{\partial^4 \bar{F}_k}{\partial \zeta_k^4} - \bar{\beta}_k^4 \bar{F}_k = 0. \tag{16}$$

The solution of the kth component is

$$\bar{F}_k = A_1^k \sin \bar{\beta}_k \zeta_k + A_2^k \cos \bar{\beta}_k \zeta_k + A_3^k \sinh \bar{\beta}_k \zeta_k + A_4^k \cosh \bar{\beta}_k \zeta_k. \tag{17}$$

The continuity conditions of different components are

$$L_k \bar{F}_k (1) = L_{k+1} \bar{F}_{k+1} (0), \tag{18}$$

$$\frac{\partial \bar{F}_k (1)}{\partial \zeta_k} = \frac{\partial \bar{F}_{k+1} (0)}{\partial \zeta_{k+1}}, \tag{19}$$

$$\frac{E_k I_k}{L_k} \frac{\partial^2 \bar{F}_k (1)}{\partial \zeta_k^2} = \frac{E_{k+1} I_{k+1}}{L_{k+1}} \frac{\partial^2 \bar{F}_{k+1} (0)}{\partial \zeta_{k+1}^2}, \tag{20}$$

$$\frac{E_k I_k}{L_k^2} \frac{\partial^3 \bar{F}_k (1)}{\partial \zeta_k^3} = \frac{E_{k+1} I_{k+1}}{L_{k+1}^2} \frac{\partial^3 \bar{F}_{k+1} (0)}{\partial \zeta_{k+1}^3}. \tag{21}$$

In this paper, the cantilevered composite sandwich beam with N components is considered. The boundary conditions are

$$\begin{cases} L_1 \bar{F}_1 (0) = 0 \\ \dfrac{\partial \bar{F}_1}{\partial \zeta_1} (0) = 0 \end{cases}, \tag{22}$$

$$\begin{cases} \dfrac{E_N I_N}{L_N} \dfrac{\partial^2 \bar{F}_N}{\partial \zeta_N^2} (1) = 0 \\ \dfrac{E_N I_N}{L_N^2} \dfrac{\partial^3 \bar{F}_N}{\partial \zeta_N^3} (1) = 0 \end{cases}. \tag{23}$$

For the nth component, the conditions at $\zeta_n = 0$ are

$$\begin{aligned} F_n (0) &= L_n \left(A_2^n + A_4^n \right) \\ \frac{\partial F_n}{\partial x_n} &= \bar{\beta}_n \left(A_1^n + A_3^n \right) \\ E_n I_n \frac{\partial^2 F_n}{\partial x_n^2} (0) &= \frac{E_n I_n}{L_n} \bar{\beta}_n^2 \left(-A_2^n + A_4^n \right) \\ E_n I_n \frac{\partial^3 F_n}{\partial x_n^3} (0) &= \frac{E_n I_n}{L_n^2} \bar{\beta}_n^3 \left(-A_1^n + A_3^n \right), \end{aligned} \tag{24}$$

and the conditions at $\zeta_n = 1$ are

$$\begin{aligned} L_n \bar{F}_n (1) &= L_n \left(A_1^n \sin \bar{\beta}_n + A_2^n \cos \bar{\beta}_n + A_3^n \sinh \bar{\beta}_n + A_4^n \cosh \bar{\beta}_n \right) \\ \frac{\partial \bar{F}_n}{\partial \zeta_n} (1) &= \bar{\beta}_n \left(A_1^n \cos \bar{\beta}_n - A_2^n \sin \bar{\beta}_n + A_3^n \cosh \bar{\beta}_n + A_4^n \sinh \bar{\beta}_n \right) \\ \frac{E_n I_n}{L_n} \frac{\partial^2 \bar{F}_n}{\partial \zeta_n^2} (1) &= \frac{E_n I_n}{L_n} \bar{\beta}_n^2 \left(-A_1^n \sin \bar{\beta}_n - A_2^n \cos \bar{\beta}_n + A_3^n \sinh \bar{\beta}_n + A_4^n \cosh \bar{\beta}_n \right) \\ \frac{E_n I_n}{L_n^2} \frac{\partial^3 \bar{F}_n}{\partial \zeta_n^3} (1) &= \frac{E_n I_n}{L_n^2} \bar{\beta}_n^3 \left(-A_1^n \cos \bar{\beta}_n + A_2^n \sin \bar{\beta}_n + A_3^n \cosh \bar{\beta}_n + A_4^n \sinh \bar{\beta}_n \right). \end{aligned} \tag{25}$$

Then, the conditions (24) and (25) can be written in matrix form as

$$\mathbf{B}^{(n)}\mathbf{A}^{(n)} = \begin{bmatrix} 0 & L_n & 0 & L_n \\ \bar{\beta}_n & 0 & \bar{\beta}_n & 0 \\ 0 & -\frac{E_nI_n}{L_n}\bar{\beta}_n^2 & 0 & \frac{E_nI_n}{L_n}\bar{\beta}_n^2 \\ -\frac{E_nI_n}{L_n^2}\bar{\beta}_n^3 & 0 & \frac{E_nI_n}{L_n^2}\bar{\beta}_n^3 & 0 \\ L_n\sin\bar{\beta}_n & L_n\cos\bar{\beta}_n & L_n\sinh\bar{\beta}_n & L_n\cosh\bar{\beta}_n \\ \bar{\beta}_n\cos\bar{\beta}_n & -\bar{\beta}_n\sin\bar{\beta}_n & \bar{\beta}_n\cosh\bar{\beta}_n & \bar{\beta}_n\sinh\bar{\beta}_n \\ -\frac{E_nI_n}{L_n}\bar{\beta}_n^2\sin\bar{\beta}_n & -\frac{E_nI_n}{L_n}\bar{\beta}_n^2\cos\bar{\beta}_n & \frac{E_nI_n}{L_n}\bar{\beta}_n^2\sinh\bar{\beta}_n & \frac{E_nI_n}{L_n}\bar{\beta}_n^2\cosh\bar{\beta}_n \\ -\frac{E_nI_n}{L_n^2}\bar{\beta}_n^3\cos\bar{\beta}_n & \frac{E_nI_n}{L_n^2}\bar{\beta}_n^3\sin\bar{\beta}_n & \frac{E_nI_n}{L_n^2}\bar{\beta}_n^3\cosh\bar{\beta}_n & \frac{E_nI_n}{L_n^2}\bar{\beta}_n^3\sinh\bar{\beta}_n \end{bmatrix} \begin{bmatrix} A_1^{(n)} \\ A_2^{(n)} \\ A_3^{(n)} \\ A_4^{(n)} \end{bmatrix}. \tag{26}$$

Taking a composite beam with 3 components as an example, the matrices **B** and **A** considering the continuity conditions and boundary conditions are written as

$$[\mathbf{B}]\,[\mathbf{A}] = \begin{bmatrix} \mathbf{B}^{(1)} & 0 & 0 \\ 0 & \mathbf{B}^{(2)} & 0 \\ 0 & 0 & \mathbf{B}^{(3)} \end{bmatrix} \begin{bmatrix} \mathbf{A}^{(1)} \\ \mathbf{A}^{(2)} \\ \mathbf{A}^{(3)} \end{bmatrix}, \tag{27}$$

where the matrix **B** is

$$\left[\begin{array}{cccc|cccc|cccc} B_{11}^{(1)} & B_{12}^{(1)} & B_{13}^{(1)} & B_{14}^{(1)} & 0 & 0 & 0 & 0 & 0 & 0 & 0 & 0 \\ B_{11}^{(1)} & B_{22}^{(1)} & B_{23}^{(1)} & B_{24}^{(1)} & 0 & 0 & 0 & 0 & 0 & 0 & 0 & 0 \\ B_{51}^{(1)} & B_{52}^{(1)} & B_{53}^{(1)} & B_{54}^{(1)} & B_{11}^{(2)} & B_{12}^{(2)} & B_{13}^{(2)} & B_{14}^{(2)} & 0 & 0 & 0 & 0 \\ B_{61}^{(1)} & B_{62}^{(1)} & B_{63}^{(1)} & B_{64}^{(1)} & B_{21}^{(2)} & B_{22}^{(2)} & B_{23}^{(2)} & B_{24}^{(2)} & 0 & 0 & 0 & 0 \\ B_{71}^{(1)} & B_{72}^{(1)} & B_{73}^{(1)} & B_{74}^{(1)} & B_{31}^{(2)} & B_{32}^{(2)} & B_{33}^{(2)} & B_{34}^{(2)} & 0 & 0 & 0 & 0 \\ B_{81}^{(1)} & B_{82}^{(1)} & B_{83}^{(1)} & B_{84}^{(1)} & B_{41}^{(2)} & B_{42}^{(2)} & B_{43}^{(2)} & B_{44}^{(2)} & 0 & 0 & 0 & 0 \\ 0 & 0 & 0 & 0 & B_{51}^{(2)} & B_{52}^{(2)} & B_{53}^{(2)} & B_{54}^{(2)} & B_{11}^{(3)} & B_{12}^{(3)} & B_{13}^{(3)} & B_{14}^{(3)} \\ 0 & 0 & 0 & 0 & B_{61}^{(2)} & B_{62}^{(2)} & B_{63}^{(2)} & B_{64}^{(2)} & B_{21}^{(3)} & B_{22}^{(3)} & B_{23}^{(3)} & B_{24}^{(3)} \\ 0 & 0 & 0 & 0 & B_{71}^{(2)} & B_{72}^{(2)} & B_{73}^{(2)} & B_{74}^{(2)} & B_{31}^{(3)} & B_{32}^{(3)} & B_{33}^{(3)} & B_{34}^{(3)} \\ 0 & 0 & 0 & 0 & B_{81}^{(2)} & B_{82}^{(2)} & B_{83}^{(2)} & B_{84}^{(2)} & B_{41}^{(3)} & B_{42}^{(3)} & B_{43}^{(3)} & B_{44}^{(3)} \\ 0 & 0 & 0 & 0 & 0 & 0 & 0 & 0 & B_{71}^{(3)} & B_{72}^{(3)} & B_{73}^{(3)} & B_{74}^{(3)} \\ 0 & 0 & 0 & 0 & 0 & 0 & 0 & 0 & B_{81}^{(3)} & B_{82}^{(3)} & B_{83}^{(3)} & B_{84}^{(3)} \end{array}\right]. \tag{28}$$

For a composite sandwich beam with N components, the matrix form is

$$[\mathbf{B}]\,[\mathbf{A}] = \begin{bmatrix} \mathbf{B}^{(1)} & \mathbf{0} & \cdots & \mathbf{0} \\ \mathbf{0} & \mathbf{B}^{(2)} & \cdots & \mathbf{0} \\ \vdots & \vdots & \ddots & \vdots \\ \mathbf{0} & \mathbf{0} & \cdots & \mathbf{B}^{(N)} \end{bmatrix} \begin{bmatrix} \mathbf{A}^{(1)} \\ \mathbf{A}^{(2)} \\ \vdots \\ \mathbf{A}^{(N)} \end{bmatrix} \tag{29}$$

To solve a non-trivial solution, the determinant of the matrix **B** in Eq. (29) should vanish as the variable ω equal to the resonant frequencies. Then, the unknown variables **A** can be determined to get the mode shapes.

3. EXPERIMENTAL METHODS AND NUMERICAL SIMULATIONS

In this study, all the specimens are made using a Mark Two Carbon Fiber 3D Printer (Markforged). The filament used is a micro-carbon fiber filled nylon (Onyx). The range of printing temperatures for Onyx and fiber are 272–275°C and 251–253°C, respectively.

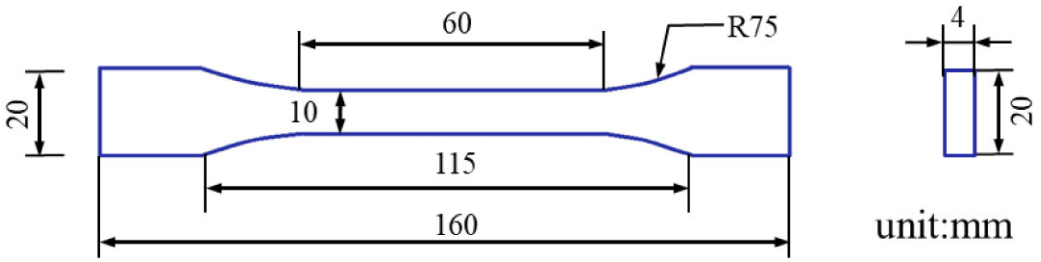

Figure 5 Configure of tensile specimen according to ISO 527-2.

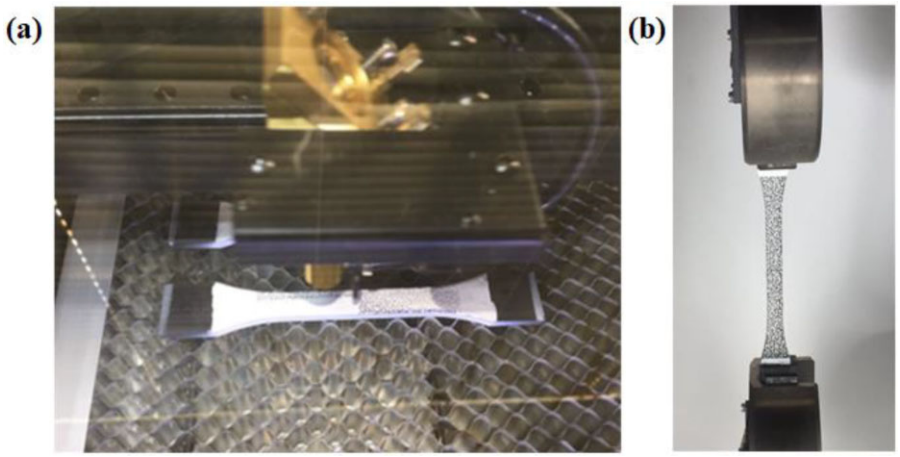

Figure 6 (a) Schematic of making speckle pattern using laser cutting machine (b) An example of tensile specimen.

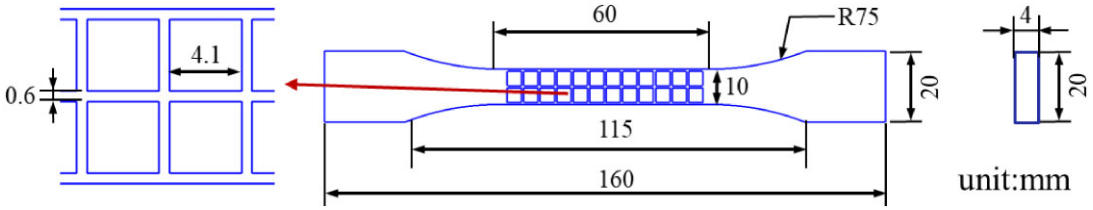

Figure 7 Configure of square grid of tensile sandwich structure.

The build and travel speeds are 55 and 120 mm/s, respectively. The solid fill pattern forms all specimens. To measure the Young's modulus and Poisson's ratio of the material, the tensile specimens according to ISO 527-2 (Fig. 5) are printed. The tensile test machine (Shimadzu AG-IS 10kN) is used with tensile speed of 4.2 mm/min. The digital image correlation (DIC) method is used to measure the true tensile strain. The specimens are sprayed with white paint. Then, the speckle pattern on the surface of the specimens is made by using a laser cutting machine (Fig. 6). The density of the material is measured using an electronic densitometer. To measure the equivalent Young's modulus of sandwich beams, 2 types of sandwich beams are made using 3D printer. One type is without filler. The other type is filled with metal mixture. The thicknesses of the face beams are 1 mm. The thickness of the core is 2 mm. The geometry of the core is as Fig. 7 shows. The metal mixture is made up of iron powder (99% near spherical 10–30 μm) and gel (Fig. 8). Due to the high number of grids and small filling areas in the sandwich beams, the time required for filling will be increased. This results in a reduction of the viscosity of the mixture, leading to uneven hole filling. After several improvements, the ratio of gel to metal powder is adjusted to 3 ml and 6.15 g, respectively. This increases the viscosity of the filler and effectively helped the metal mixture adhere to the grids, reducing the detachment of the mixture from the sandwich beam during the subsequent printing process due to external forces. To make the sandwich beams filled with metal mixture, the bottom beam and square grids are printed first. After filling the metal mixture into the core, the top beam is printed. Then, the speckle pattern is made. At last, the tensile test is conducted as Fig. 9 shows.

To measure the natural frequencies and mode shapes of the sandwich structures, the amplitude-fluctuation electronic speckle pattern interferometer (AF-ESPI) is used, as Fig. 10 shows. The Helium-neon laser (Pacific Lasertec) with wavelength 633 nm and power 35 mW is used. The shaker (Data Physics, GW-V4) connected to the power amplifier (Data Physics, PA30E) and function generator (Keysight, 33210A) is used to excite the specimen. The CCD (Allied Vision, PIKEF-505c) is used to capture the figures. In this study, 4 types of cantilevered uniform sandwich beams are made as Fig. 11 shows. The length of the fixture part is 25 mm. The size

Figure 8 Iron powder (99% near spherical 10–30 μm) and gel.

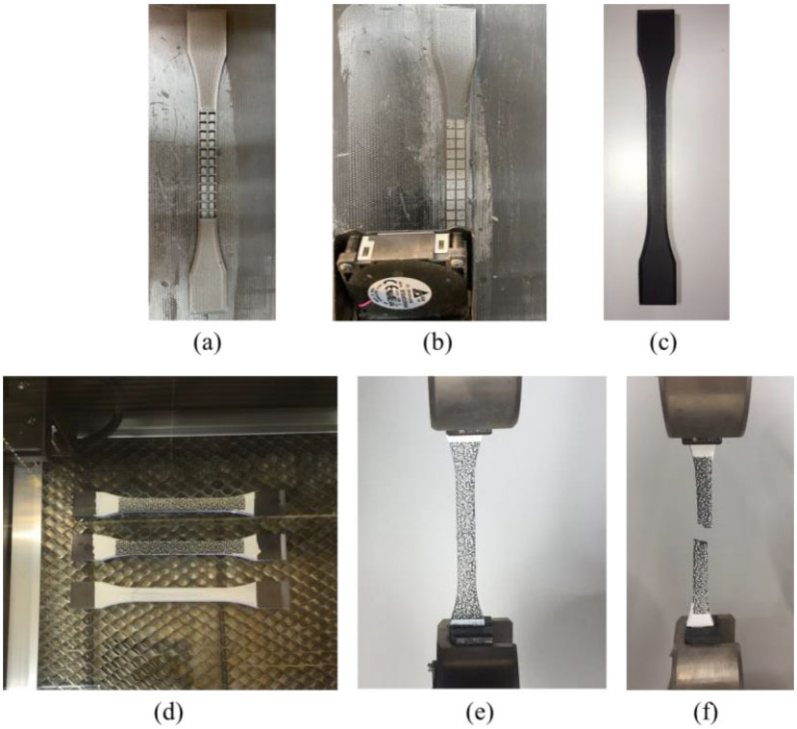

Figure 9 Procedure of making sandwich beams filled with metal mixture (a) Bottom beam and square grid core (b) Filling metal mixture (c) Sandwich beam (d) Making speckle pattern using laser cutting machine (e) Tensile test (f) Broken specimen.

parameters of the 4 types of sandwich beams are shown in Table 1. In the experiments, the sandwich beams filled without and with metal mixture are considered.

The finite element software ABAQUS is used to simulate the vibration of sandwich beams. The element type C3D20R is used. The convergence tests of the 4 types of sandwich beams are conducted with different mesh sizes as Table 2 shows. Since the size of 0.3 mm is too small, the calculations of types 2 and 4 are aborted. To ensure convergence, the element size 0.5 mm is used. For the equivalent model, the equivalent parameters are used in the simulation. To simulate the detailed models of sandwich beams, the experimental material parameters are used. To simulate the detailed models of sandwich beams filled with metal mixture, the mass of the metal mixture is equally added to each square as a non-structural mass.

Two types of composite sandwich beams are considered. The composite sandwich beams consist of type 2 and 4. Figure 12 shows the schematic of a composite sandwich beam with 3 blocks. The total length is 198.8 mm. Figure 13 shows the schematic of a composite sandwich beam with 4 blocks. The total length is 200 mm. The detailed size parameters of the two composite sandwich beams are listed in Table 3. For each type of sandwich beams, 3 specimens are printed, and 2 modal experiments are conducted for each specimen.

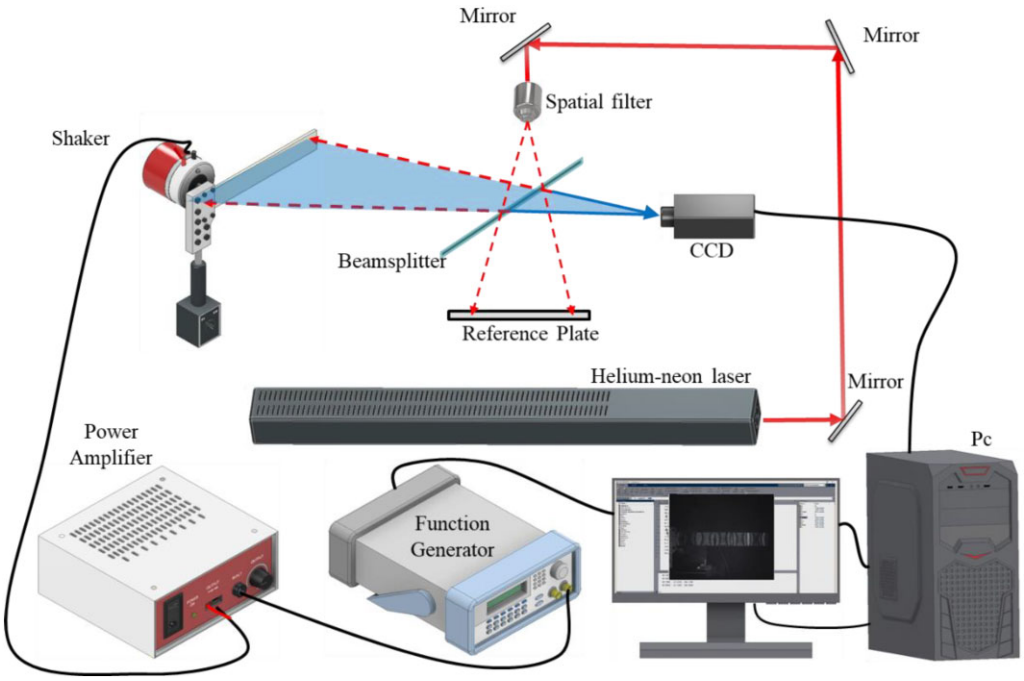

Figure 10 Schematic of experimental setup of AF-ESPI

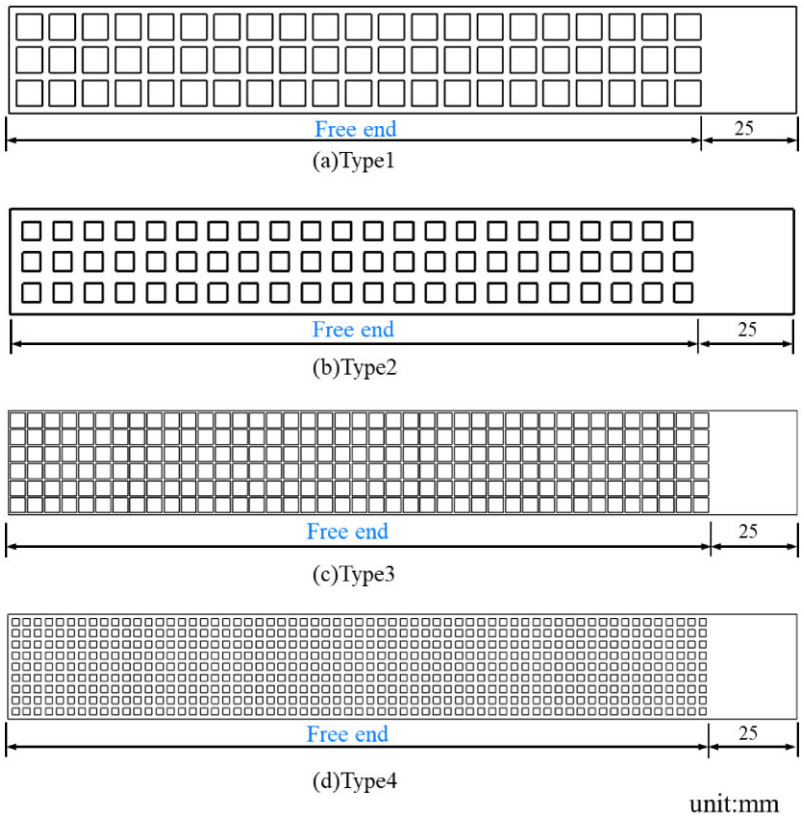

Figure 11 Four types of cantilevered uniform sandwich beams.

4. RESULTS AND DISCUSSION

Figure 14 shows experimental stress-strain curves of 3 tensile tests of Onyx. The average Young's modulus and Poisson's ratio are 1.133 GPa and 0.471, respectively. The measured density is 1092.67 kg/m^3. The measured material properties are used in the

Table 1 Size parameters of 4 types of sandwich beams.

Unit: (mm)	Type 1	Type 2	Type 3	Type 4
Length (L)	197.4	197.2	201.5	202.8
Width (b)	30	30	30	30
Total thickness (H)	3	3	3	3
Cover thickness (t_f)	0.6	0.6	0.6	0.6
Core thickness (h_c)	1.8	1.8	1.8	1.8
Grid spacing (s)	7.2	5.2	4.3	2
Square wall width (t_2)	2.1	3.6	0.6	1.2
Number of grids	3 × 21	3 × 22	6 × 41	9 × 63

Table 2 Convergence tests of 4 types of sandwich beams.

Mesh (mm)	0.3	0.5	0.8	1	0.3	0.5	0.8	1
Mode	Type 1 Natural Frequency (Hz)				Type 2 Natural Frequency (Hz)			
1	14.637	14.637	14.645	14.641	-	13.724	13.731	13.733
2	91.219	91.219	91.279	91.241	-	85.702	85.747	85.763
3	254.24	254.23	254.44	254.3	-	239.64	239.78	239.83
4	495.29	495.24	495.78	495.36	-	469.12	469.43	469.55
5	811.9	811.73	812.88	811.94	-	773.9	774.54	774.74
6	1198.7	1198.2	1200.3	1198.4	-	1151.5	1152.7	1153.1
7	1648.5	1647.6	1651.4	1648.2	-	1598.2	1600.2	1600.9
8	2153.1	2151.6	2156.8	2152.3	-	2109	2112	2113
9	2702.5	2700.1	2709.6	2700.8	-	2676.7	2681	2682.6
10	3277.5	3274.1	3286.3	3275.8	-	3282.8	3288.9	3290.8
Mode	Type 3 Natural Frequency (Hz)				Type 4 Natural Frequency (Hz)			
1	15.125	15.128	15.148	15.152	-	13.122	13.124	13.125
2	94.249	94.275	94.421	94.454	-	82.005	82.021	82.021
3	262.49	262.58	263.09	263.21	-	229.47	229.49	229.54
4	510.77	511.04	512.29	512.5	-	449.71	449.8	449.84
5	836.21	836.8	839.42	840.32	-	743.1	743.33	743.33
6	1233	1234.2	1239.1	1240.8	-	1108.1	1108.6	1108.5
7	1694	1696	1704.2	1707.4	-	1542.2	1543.1	1542.7
8	2211	2214.1	2227.1	2230.6	-	2041.7	2043.2	2042.5
9	2775	2780.3	2798.9	2805.7	-	2601.7	2603.9	2602.7
10	3374.5	3381.5	3407.6	3417.4	-	3212.9	3216	3214.2

following numerical models. Figure 15 shows experimental stress-strain curves of 3 sandwich beams as Fig. 7 shows. Figure 16 shows experimental stress-strain curves of 3 sandwich beams filled with metal mixture. The average equivalent Young's modulus of sandwich beams is 1.031 GPa. And the average equivalent Young's modulus of sandwich beams filled with metal mixture is 1.128 GPa. This means that the metal mixture has little effect on the equivalent Young's modulus. It only has mass effect on the structure. Thus, it is possible to change the equivalent density with almost constant stiffness of sandwich beams by filling metal mixture into the cores.

Table 4 shows the measured masses of 4 types of sandwich beams filled without and with metal mixture. "Hollow" means the sandwich beams filled without metal mixture. "Filled" means the sandwich beams filled with metal mixture. Table 5 shows the equivalent parameters of 4 types of sandwich beams filled without and with metal mixture. Table 6 shows the first 10 numerical natural frequencies of 4 types of sandwich beams filled without and with metal mixture using detailed simulations. Table 7 shows the first 10 numerical natural frequencies of 4 types of sandwich beams filled without and with metal mixture using equivalent simulations. Figure 17 shows the first 10 numerical natural frequencies of 4 types of sandwich beams filled without and with metal mixture. As shown in Fig. 17(a) and (c), the differences of natural frequencies between detailed simulations and equivalent simulations increase as the frequency increases. The differences in natural frequencies between detailed simulations and equivalent simulations for types 2 and 4 are much smaller than those for types 1 and 3. It indicates that the equivalent simulation method is suitable for square grid cores with low void ratio such as types 2 and 4. Table 8 shows first 10 theoretical natural frequencies of 4 types of sandwich beams filled without and with metal mixture.

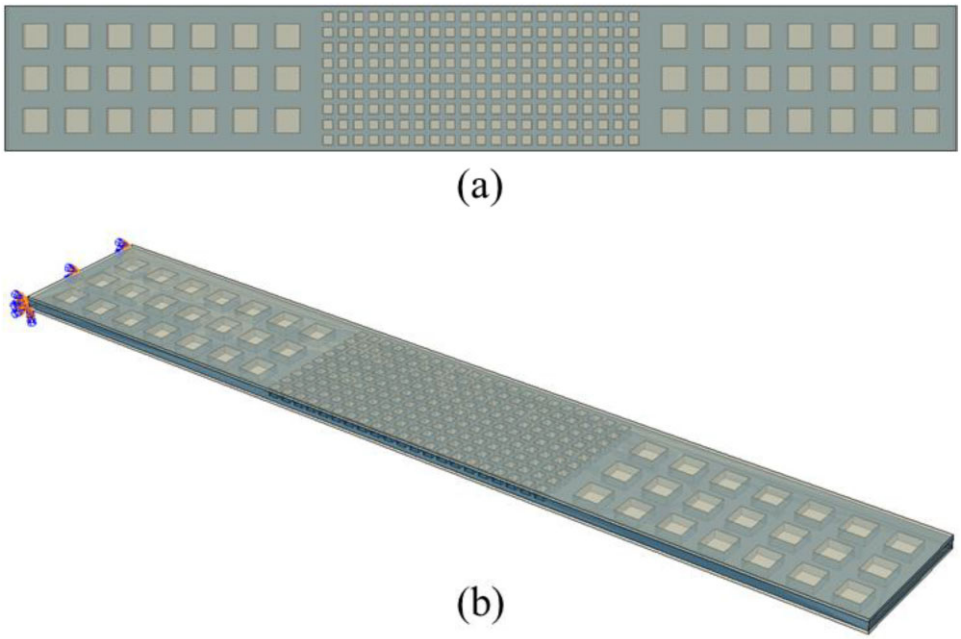

Figure 12 Schematic of a composite sandwich beam with 3 blocks (a) Top view (b) Three view.

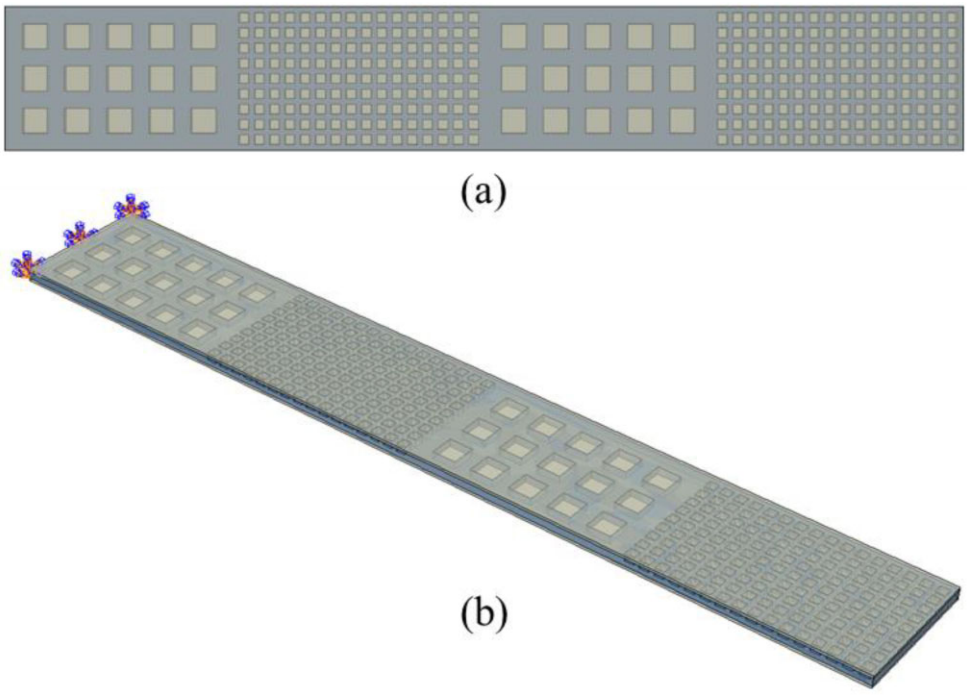

Figure 13 Schematic of a composite sandwich beam with four blocks (a) Top view (b) Three view

Figures 18–21 show the first 10 experimental and numerical mode shapes of 4 types of sandwich beams without metal mixture. "Square Sandwich" means the numerical results of the detailed models of sandwich beams. "Equivalent" means the numerical results of the equivalent model. It has been found that third natural frequencies have the maximum differences between experimental and numerical results. The maximum differences of the 4 types are 33.74, 34.39, 21.87 and 31.05%. The natural frequency of the torsion mode is close to the natural frequency of the third bending mode, thus, when measuring the mode shape of the third mode, the torsion mode affects it. For example, the numerical third natural frequency of type 2 is 236.63 Hz. The measured natural frequency of the first torsion mode is 237 Hz. Figures 22–25 show the first 10 experimental and numerical mode shapes of 4 types of sandwich

Table 3 Size parameters of two composite sandwich beams.

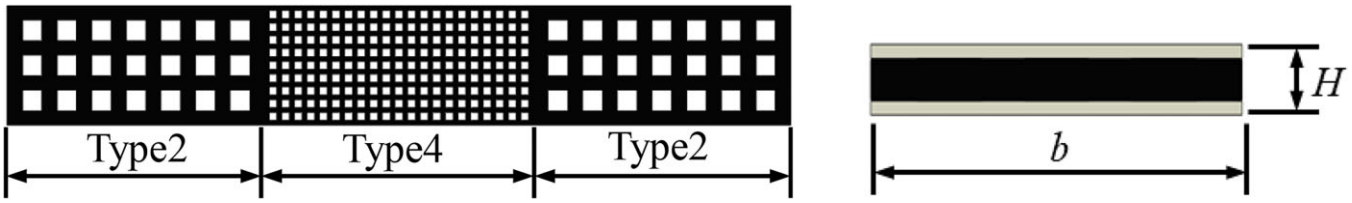

Unit: (mm)	Length (L)	Width (b)	Total thickness (H)	Cover thickness (t_f)
Type 2	65.2	30	3	0.6
Type 4	68.4	30	3	0.6

Square grid core

Unit: (mm)	Core thickness (h_c)	Grid spacing (s)	Square wall width (t_2)	Number of grids ($m \times n$)
Type 2	1.8	5.2	3.6	3×7
Type 4	1.8	2	1.2	9×21

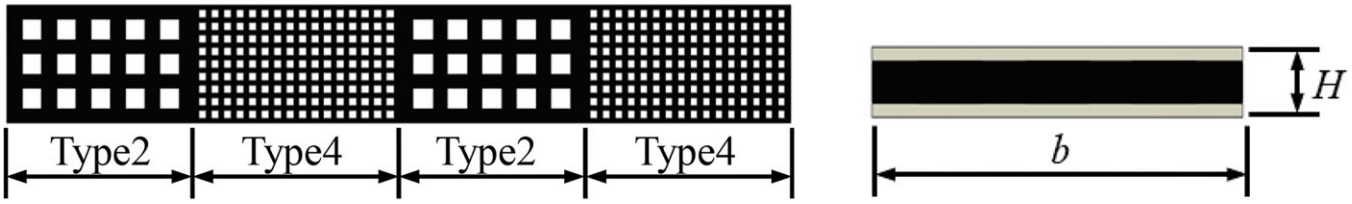

Unit: (mm)	Length (L)	Width (b)	Total thickness (H)	Cover thickness (t_f)
Type 2	47.6	30	3	0.6
Type 4	52.4	30	3	0.6

Square grid core

Unit: (mm)	Core thickness(h_c)	Grid spacing (s)	Square wall width (t_2)	Number of grids ($m \times n$)
Type 2	1.8	5.2	3.6	3×5
Type 4	1.8	2	1.2	9×16

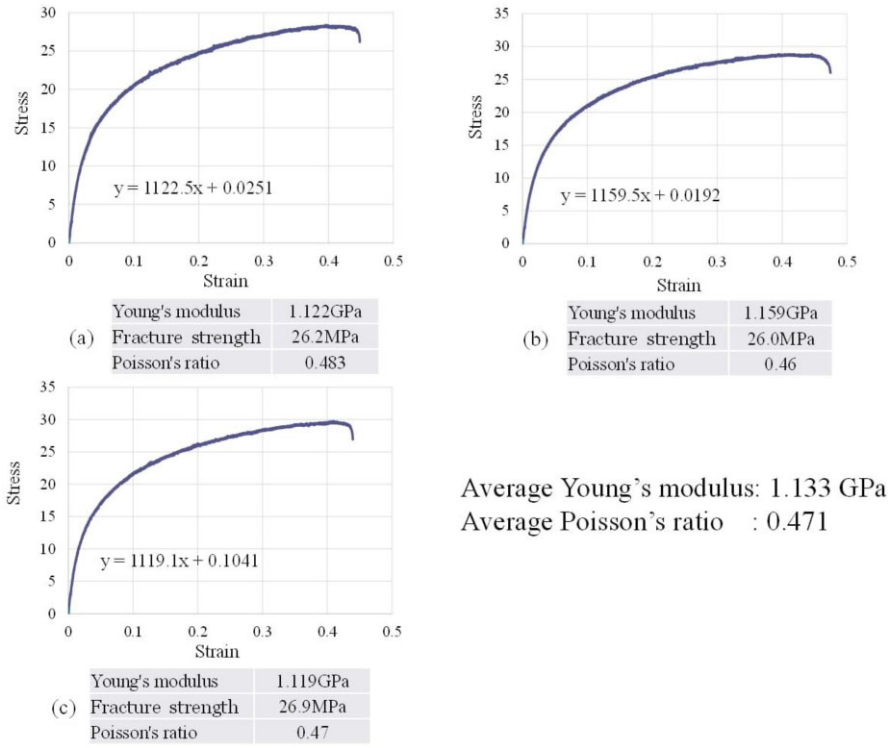

Figure 14 Experimental stress-strain curves of 3 tensile tests of Onyx.

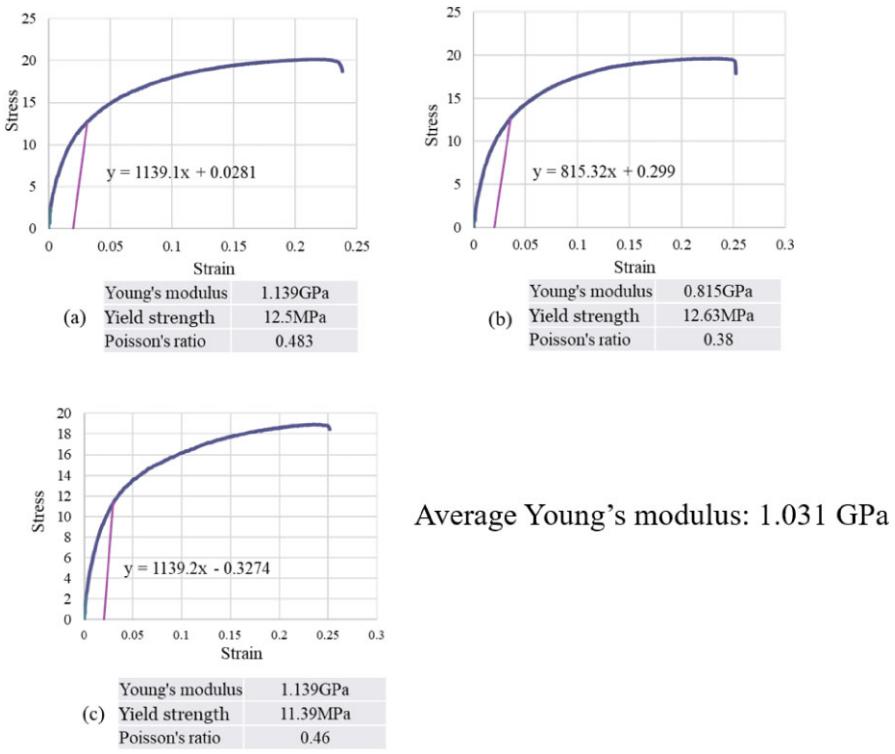

Figure 15 Experimental stress-strain curves of 3 sandwich beams.

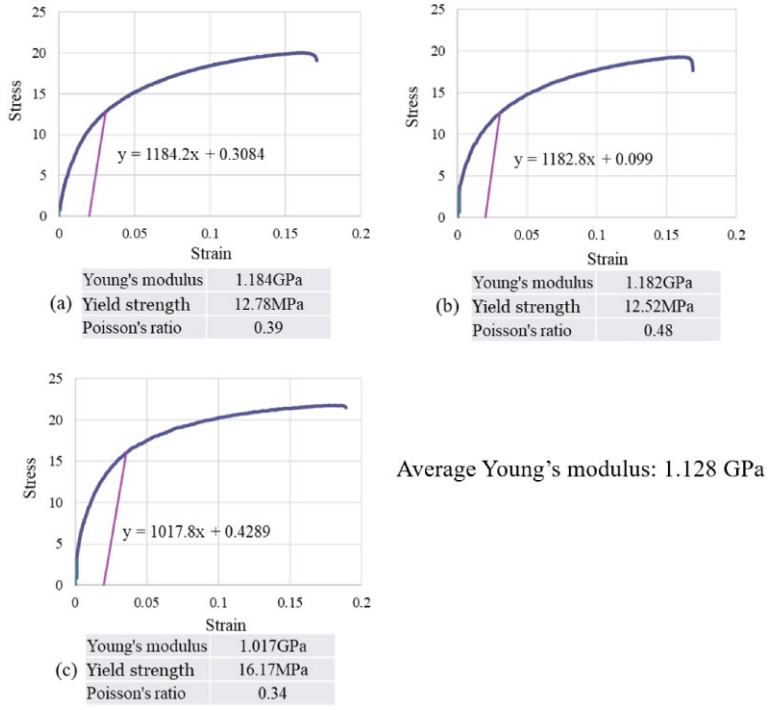

Figure 16 Experimental stress-strain curves of 3 sandwich beams filled with metal mixture.

beams filled with metal mixture. It is found that only first 6 mode shapes of type 1 and type 3 can be measured. The higher modes cannot be measured. The metal mixture in the square grid affects the vibration of the sandwich beams with a high void ratio. The first 8 mode shapes can be measured for type 2. And the first 10 mode shapes can be measured for type 4. From the experiments, it can be concluded that the density of the sandwich beam can be increased by filling with the metal mixture with almost constant stiffness, which offers a method to control the vibration characteristics.

Table 4 Mass of sandwich beams filled without and with metal mixture.

Unit:(g)	Type1	Type2	Type3	Type4
Hollow	15.64	19.235	14.545	18.018
Filled	27.45	23.746	28.54	23.96
Increased mass	11.81	4.511	13.995	5.942

Table 5 Equivalent parameters of four types of sandwich beams.

	H_{eq} (mm)	E_{eq} (GPa)	ρ_{eq} (kg/m^3) Without filler	ρ_{eq} (kg/m^3) With filler
Type 1	3.6579	0.5279	599.6010	1144.7808
Type 2	3.4077	0.6865	787.8412	1011.6048
Type 3	3.8911	0.4229	462.1002	1057.0794
Type 4	3.4986	0.6220	727.3867	1006.5465

Table 6 Numerical natural frequencies of 4 types of sandwich beams filled without and with metal mixture using detailed simulations.

	Type 1 (Hz)			Type 2 (Hz)		
Mode	Hollow	Filled	Diff. (%)	Hollow	Filled	Diff. (%)
1	14.64	10.60	27.57	13.72	12.11	11.79
2	91.22	66.07	27.57	85.70	75.60	11.79
3	254.23	184.19	27.55	239.64	211.36	11.80
4	495.24	358.91	27.53	469.12	413.70	11.81
5	811.73	588.53	27.50	773.90	682.35	11.83
6	1198.20	869.21	27.46	1151.50	1015.20	11.84
7	1647.60	1195.90	27.42	1598.20	1408.70	11.86
8	2151.60	1562.80	27.37	2109.00	1858.70	11.87
9	2700.10	1962.50	27.32	2676.70	2358.50	11.89
10	3274.10	2381.00	27.28	3282.80	2890.90	11.94
	Type 3 (Hz)			Type 4 (Hz)		
Mode	Hollow	Filled	Diff. (%)	Hollow	Filled	Diff. (%)
1	15.13	9.98	34.01	13.12	11.16	14.99
2	94.28	62.20	34.02	82.01	69.71	14.99
3	262.58	173.17	34.05	229.47	195.07	14.99
4	511.04	336.80	34.10	449.71	382.30	14.99
5	836.80	551.11	34.14	743.10	631.70	14.99
6	1234.20	812.27	34.19	1108.10	941.99	14.99
7	1696.00	1115.60	34.22	1542.20	1311.00	14.99
8	2214.10	1455.70	34.25	2041.70	1735.60	14.99
9	2780.30	1826.90	34.29	2601.70	2211.70	14.99
10	3381.50	2219.60	34.36	3212.90	2731.30	14.99

Figure 26 shows a comparison of theoretical and numerical mode shapes of composite sandwich beams with 3 blocks filled without metal mixture. "Theory" means the theoretical results obtained by using Eq. (29). The differences of natural frequencies between "Equivalent" and "Square Sandwich" are smaller than 2%. The maximum difference of the natural frequencies between "Theory" and "Square Sandwich" is −3.75% for the first mode. Figure 27 shows a comparison of theoretical and numerical mode shapes of composite sandwich beams with 4 blocks filled without metal mixture. The differences of natural frequencies between "Equivalent" and "Square Sandwich" are smaller than 2%. The maximum difference of the natural frequencies between "Theory" and "Square Sandwich" is −3.70% for the first mode. Table 9 shows the numerical natural frequencies of two composite sandwich beams filled without and with metal mixture using detailed simulations. Table 10 shows the numerical natural frequencies of two composite sandwich beams filled without and with metal mixture using equivalent simulations. Table 11 shows the experimental natural frequencies of two composite sandwich beams filled without and with metal mixture using equivalent simulations. It can be seen that the natural frequencies of a composite sandwich beam with 3 blocks decrease by about 14% by filling in the metal mixture. And the natural frequencies of composite sandwich beam with 4 blocks decrease by about 16% by filling in the metal mixture. Table 12 shows a comparison of

Table 7 Numerical natural frequencies of 4 types of sandwich beams filled without and with metal mixture using equivalent simulations.

	Type 1 (Hz)			Type 2 (Hz)		
Mode	**Hollow**	**Filled**	**Diff. (%)**	**Hollow**	**Filled**	**Diff. (%)**
1	14.55	10.53	27.64	13.52	11.93	11.77
2	90.93	65.80	27.64	84.49	74.46	11.88
3	254.56	184.20	27.64	236.63	208.77	11.77
4	499.20	361.22	27.64	464.32	409.65	11.77
5	825.46	597.30	27.64	768.38	677.91	11.77
6	1231.90	891.38	27.64	1147.80	1012.60	11.78
7	1715.80	1241.50	27.64	1600.30	1411.80	11.78
8	2273.20	1644.90	27.64	2122.70	1872.70	11.78
9	2898.50	2097.30	27.64	2709.90	2390.70	11.78
10	3577.70	2588.80	27.64	3348.90	2954.50	11.78
	Type 3 (Hz)			Type 4 (Hz)		
Mode	Hollow	Filled	Diff. (%)	Hollow	Filled	Diff. (%)
1	15.13	10.00	33.89	12.99	11.04	15.01
2	94.58	62.52	33.89	81.21	69.02	15.01
3	264.67	174.97	33.89	227.40	193.27	15.01
4	518.75	342.93	33.89	446.14	379.16	15.01
5	857.27	566.71	33.89	738.21	627.38	15.01
6	1278.50	845.17	33.89	1102.60	937.08	15.01
7	1779.50	1176.40	33.89	1537.40	1306.60	15.01
8	2356.10	1557.50	33.89	2039.60	1733.30	15.02
9	3002.60	1984.90	33.89	2604.80	2213.60	15.02
10	3707.70	2451.00	33.89	3224.30	2740.10	15.02

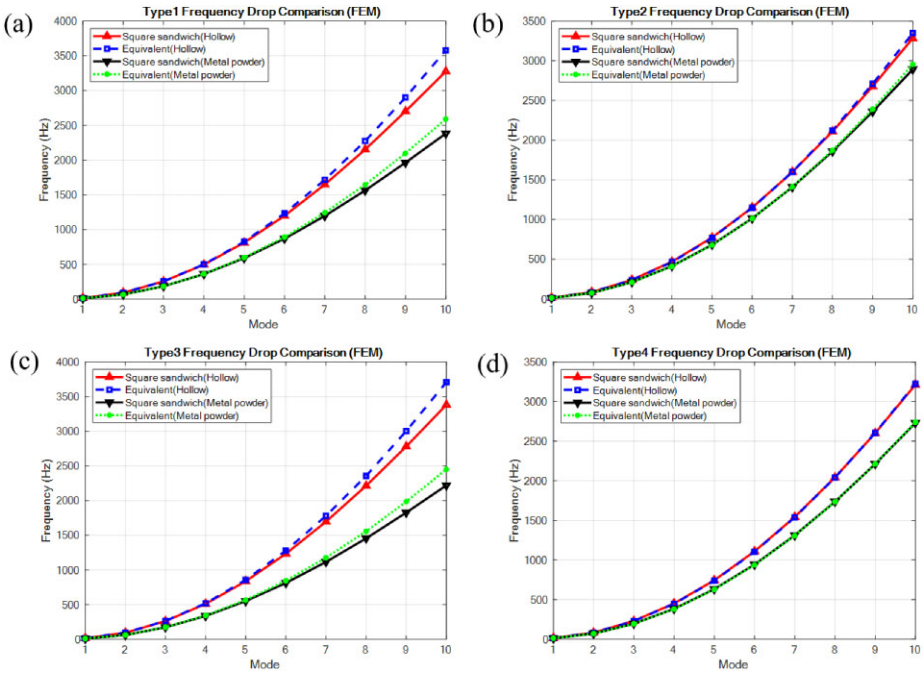

Figure 17 First 10 numerical natural frequencies of 4 types of sandwich beams filled without and with metal mixture.

experimental and theoretical natural frequencies of two composite sandwich beams filled with metal mixture. It proves that the developed equivalent theory can predict the natural frequencies of composite sandwich beams accurately. Figure 28 shows the comparison of experimental and numerical mode shapes of composite sandwich beams with 3 blocks filled without metal mixture. Figure 29 shows the comparison of experimental and numerical mode shapes of composite sandwich beams with 4 blocks filled without metal

Table 8 Theoretical natural frequencies of four types of sandwich beams filled without and with metal mixture.

	Type 1 (Hz)			Type 2 (Hz)		
Mode	**Hollow**	**Filled**	**Diff. (%)**	**Hollow**	**Filled**	**Diff. (%)**
1	14.22	10.3	27.57	13.21	11.66	11.73
2	89.17	64.54	27.62	82.80	73.08	11.74
3	249.7	180.71	27.63	231.88	204.61	11.76
4	489.24	354.11	27.62	454.32	400.96	11.75
5	808.59	585.37	27.61	750.86	662.82	11.73
6	1207.74	874.45	27.60	1121.50	990.14	11.71
7	1686.69	1221.34	27.59	1566.20	1382.92	11.70
8	2245.45	1626.04	27.59	2085.15	1841.17	11.70
9	2884.02	2088.56	27.58	2678.10	2364.88	11.70
10	3602.38	2608.89	27.58	3345.20	2954.05	11.69
	Type 3 (Hz)			Type 4 (Hz)		
Mode	Hollow	Filled	Diff. (%)	Hollow	Filled	Diff. (%)
1	14.80	9.79	33.85	12.70	10.8	14.96
2	92.81	61.37	33.88	79.62	67.69	14.98
3	259.89	171.83	33.88	222.98	189.55	14.99
4	509.21	336.71	33.88	436.89	371.44	14.98
5	841.59	556.61	33.86	722.06	614.01	14.96
6	1257.00	831.48	33.85	1078.50	917.23	14.95
7	1755.50	1161.32	33.85	1506.20	1281	14.95
8	2337.10	1546	33.85	2005.20	1705.59	14.94
9	3001.72	1985.92	33.84	2575.40	2190.73	14.94
10	3749.40	2480.69	33.84	3216.90	2736.52	14.93

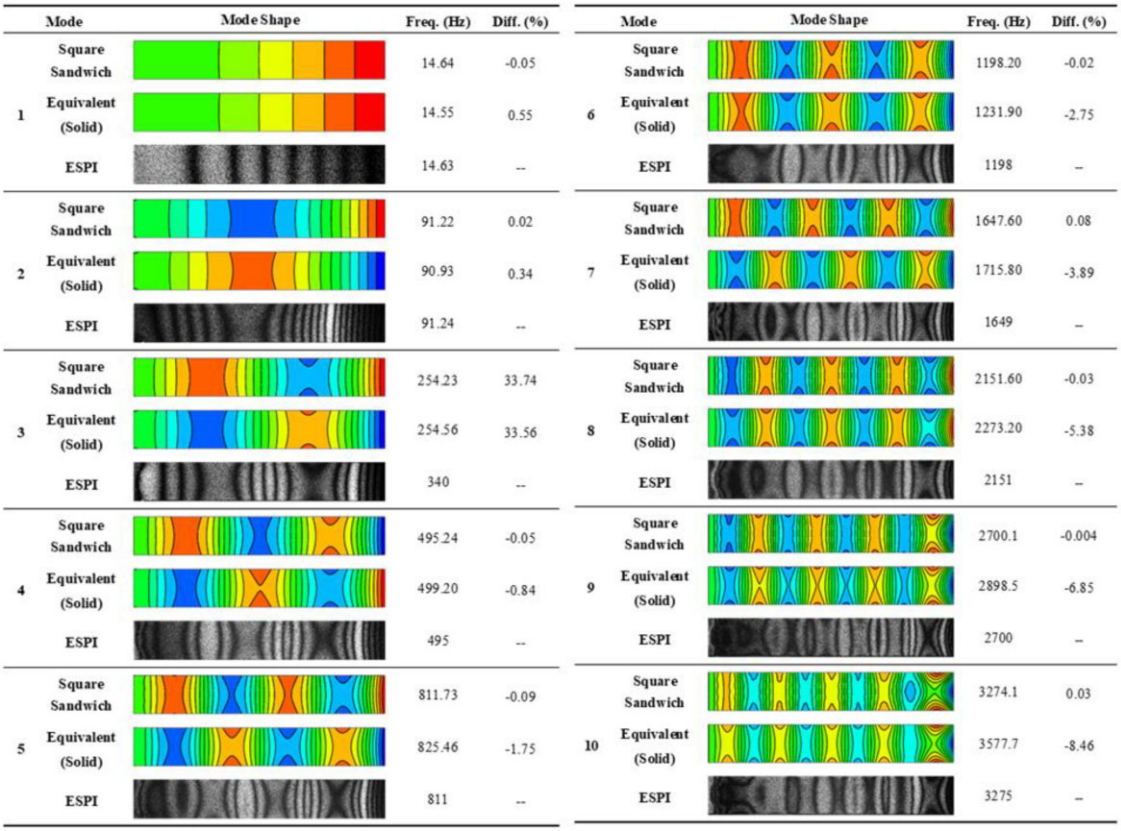

Figure 18 Comparison of numerical and experimental mode shapes of sandwich beams without metal mixture for type 1.

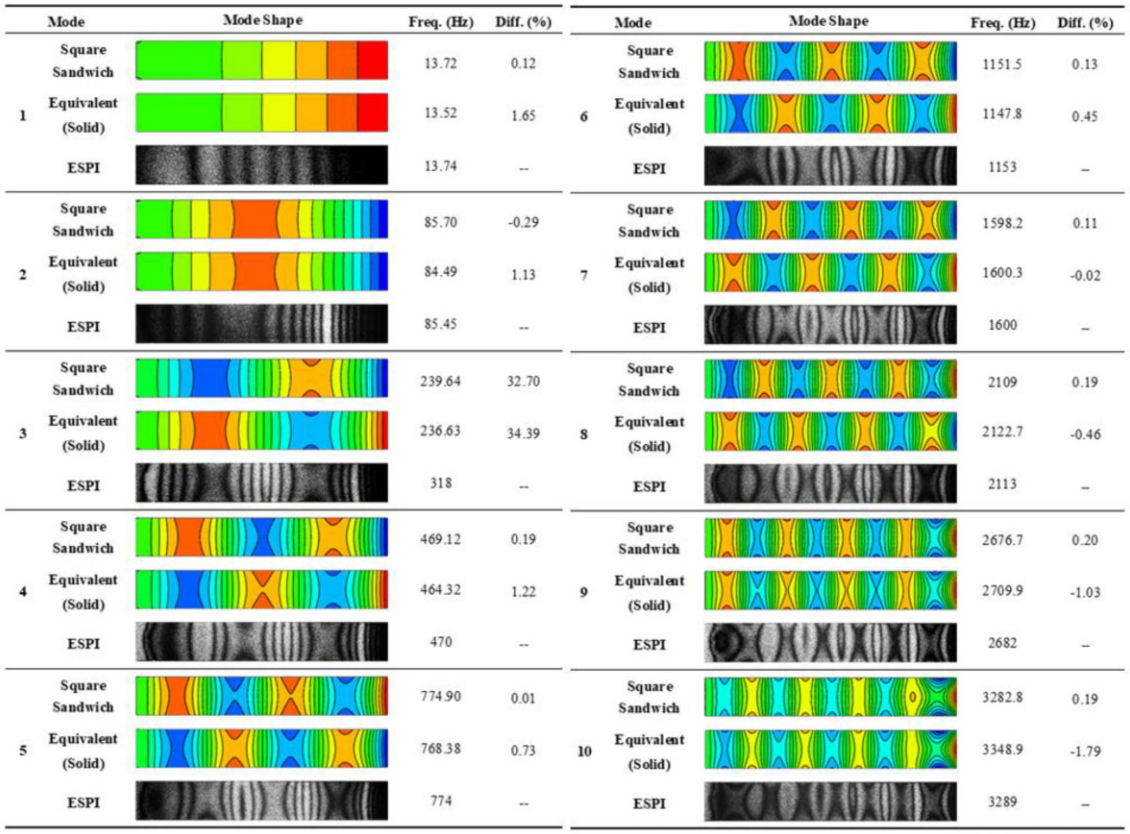

Figure 19 Comparison of numerical and experimental mode shapes of sandwich beams without metal mixture for type 2.

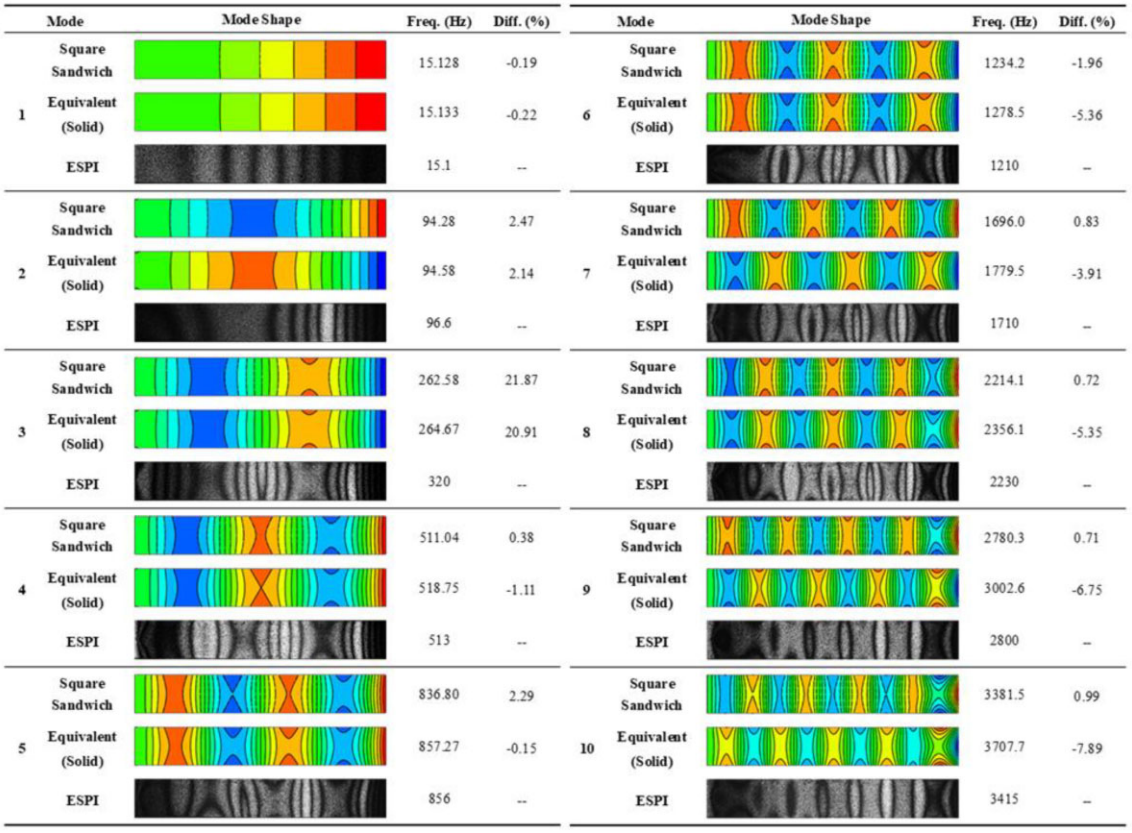

Figure 20 Comparison of numerical and experimental mode shapes of sandwich beams without metal mixture for type 3.

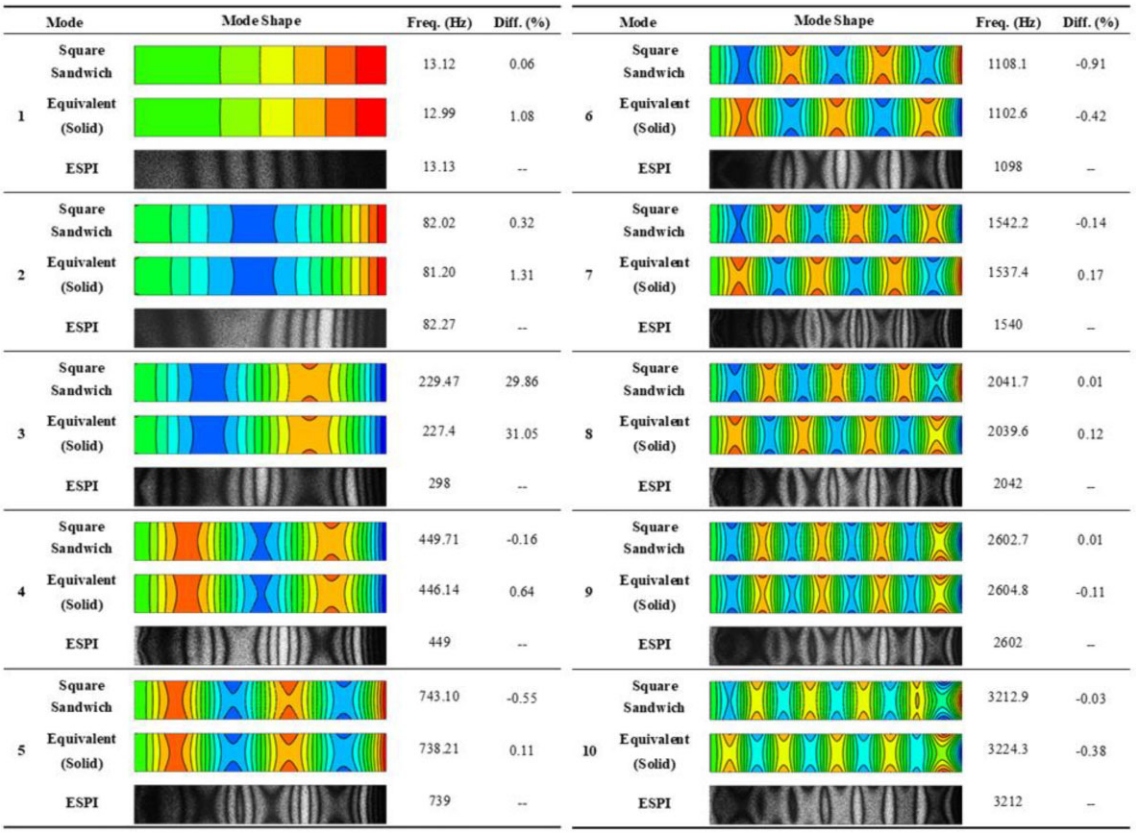

Figure 21 Comparison of numerical and experimental mode shapes of sandwich beams without metal mixture for type 4.

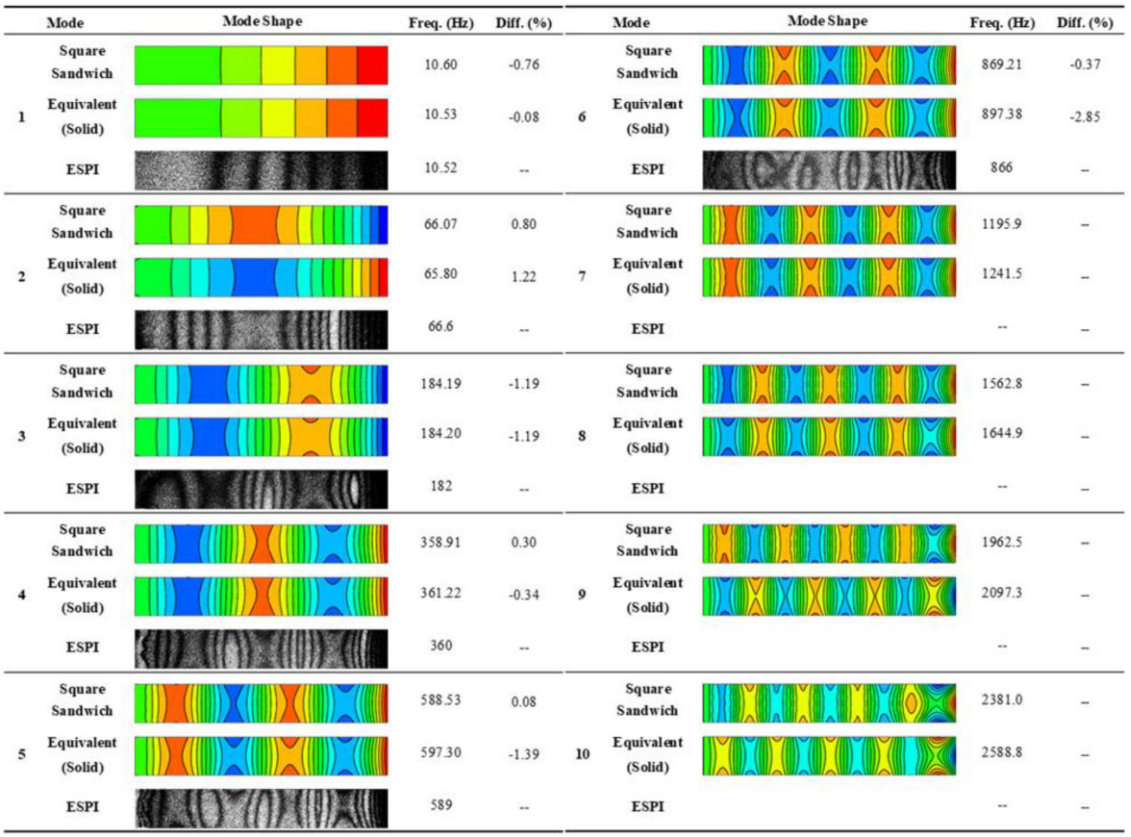

Figure 22 Comparison of numerical and experimental mode shapes of sandwich beams filled with metal mixture for type 1.

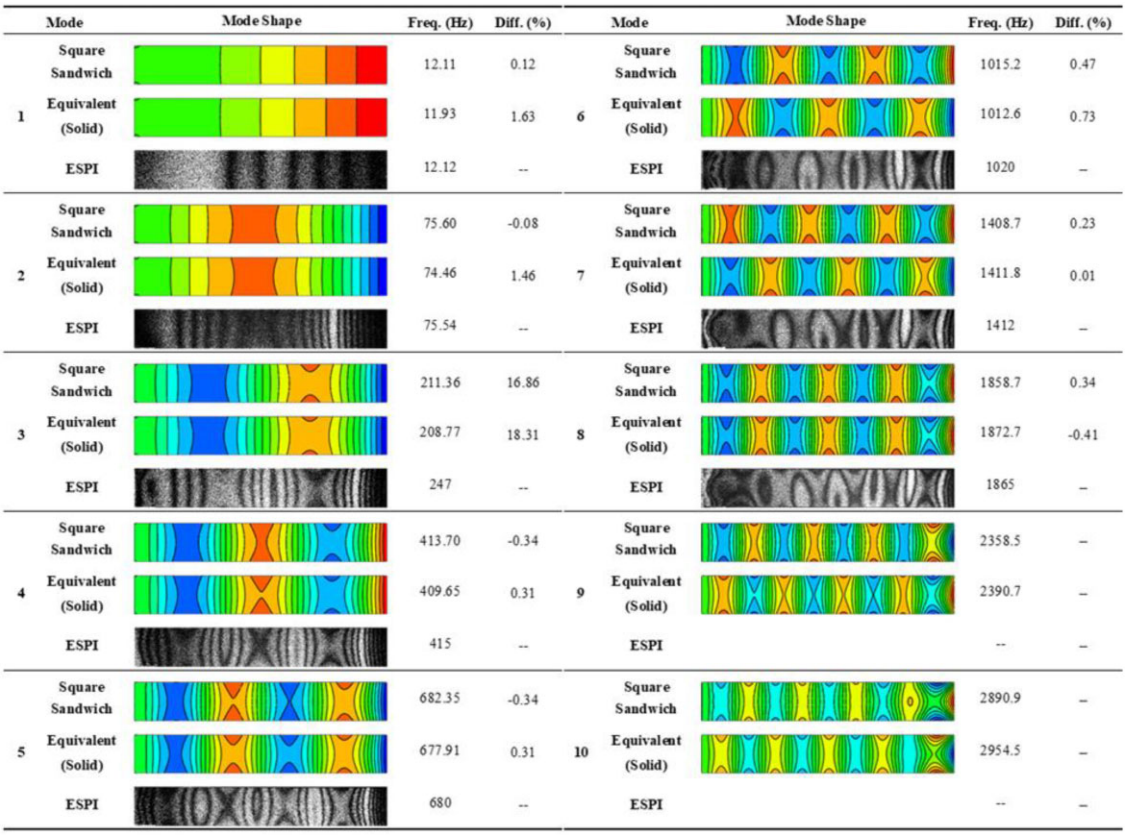

Figure 23 Comparison of numerical and experimental mode shapes of sandwich beams filled with metal mixture for type 2.

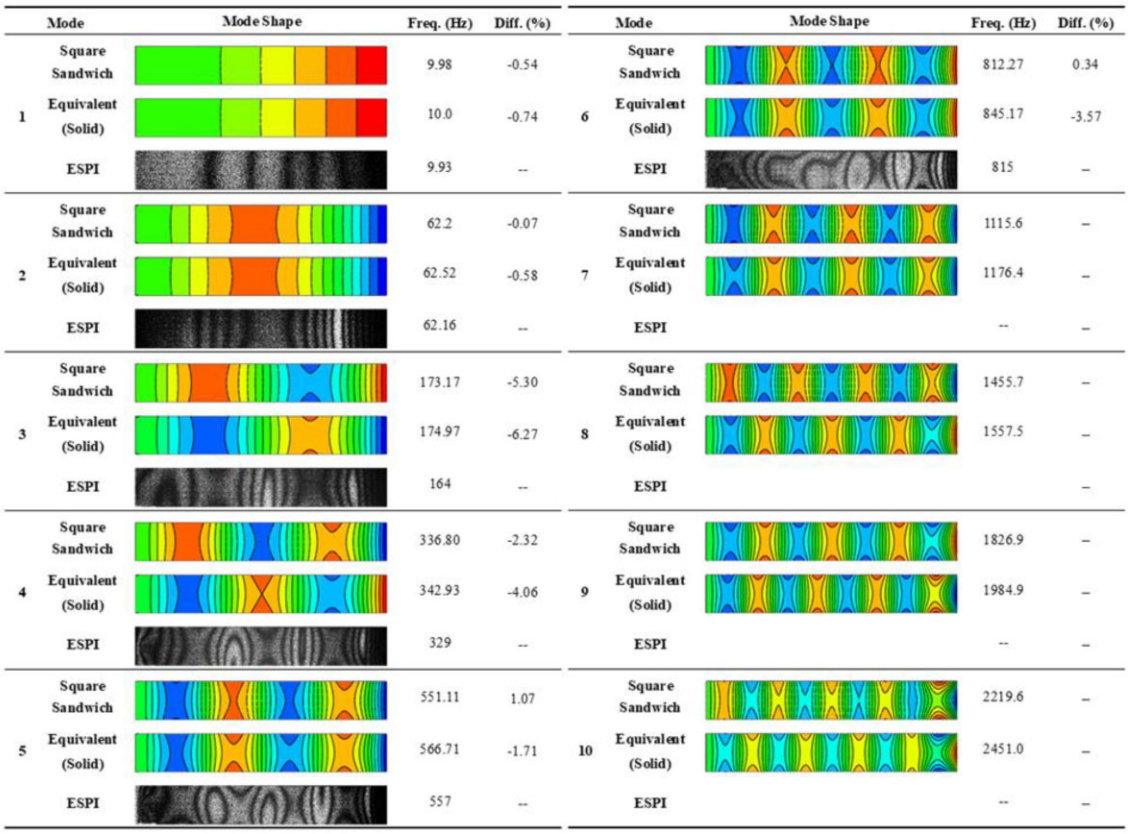

Figure 24 Comparison of numerical and experimental mode shapes of sandwich beams filled with metal mixture for type 3.

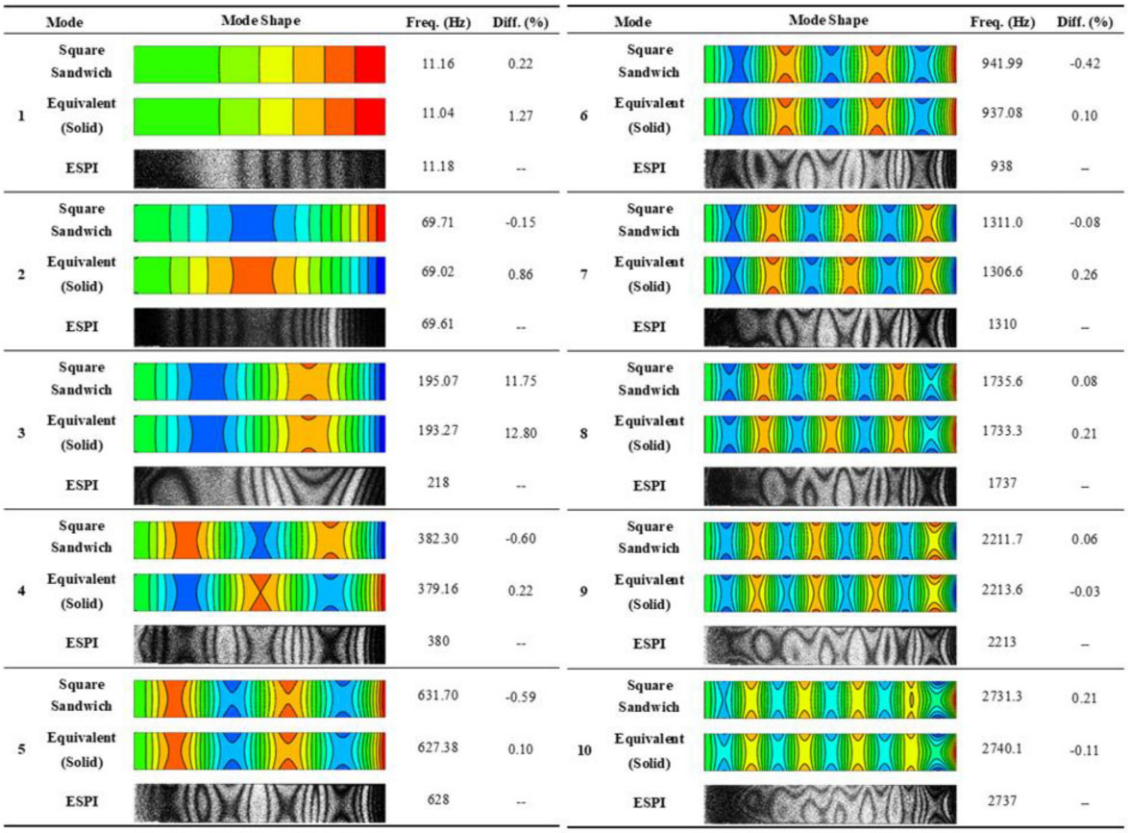

	Mode	Mode Shape	Freq. (Hz)	Diff. (%)
1	Square Sandwich		11.16	0.22
	Equivalent (Solid)		11.04	1.27
	ESPI		11.18	--
2	Square Sandwich		69.71	-0.15
	Equivalent (Solid)		69.02	0.86
	ESPI		69.61	--
3	Square Sandwich		195.07	11.75
	Equivalent (Solid)		193.27	12.80
	ESPI		218	--
4	Square Sandwich		382.30	-0.60
	Equivalent (Solid)		379.16	0.22
	ESPI		380	--
5	Square Sandwich		631.70	-0.59
	Equivalent (Solid)		627.38	0.10
	ESPI		628	--

	Mode	Mode Shape	Freq. (Hz)	Diff. (%)
6	Square Sandwich		941.99	-0.42
	Equivalent (Solid)		937.08	0.10
	ESPI		938	--
7	Square Sandwich		1311.0	-0.08
	Equivalent (Solid)		1306.6	0.26
	ESPI		1310	--
8	Square Sandwich		1735.6	0.08
	Equivalent (Solid)		1733.3	0.21
	ESPI		1737	--
9	Square Sandwich		2211.7	0.06
	Equivalent (Solid)		2213.6	-0.03
	ESPI		2213	--
10	Square Sandwich		2731.3	0.21
	Equivalent (Solid)		2740.1	-0.11
	ESPI		2737	--

Figure 25 Comparison of numerical and experimental mode shapes of sandwich beams filled with metal mixture for type 4.

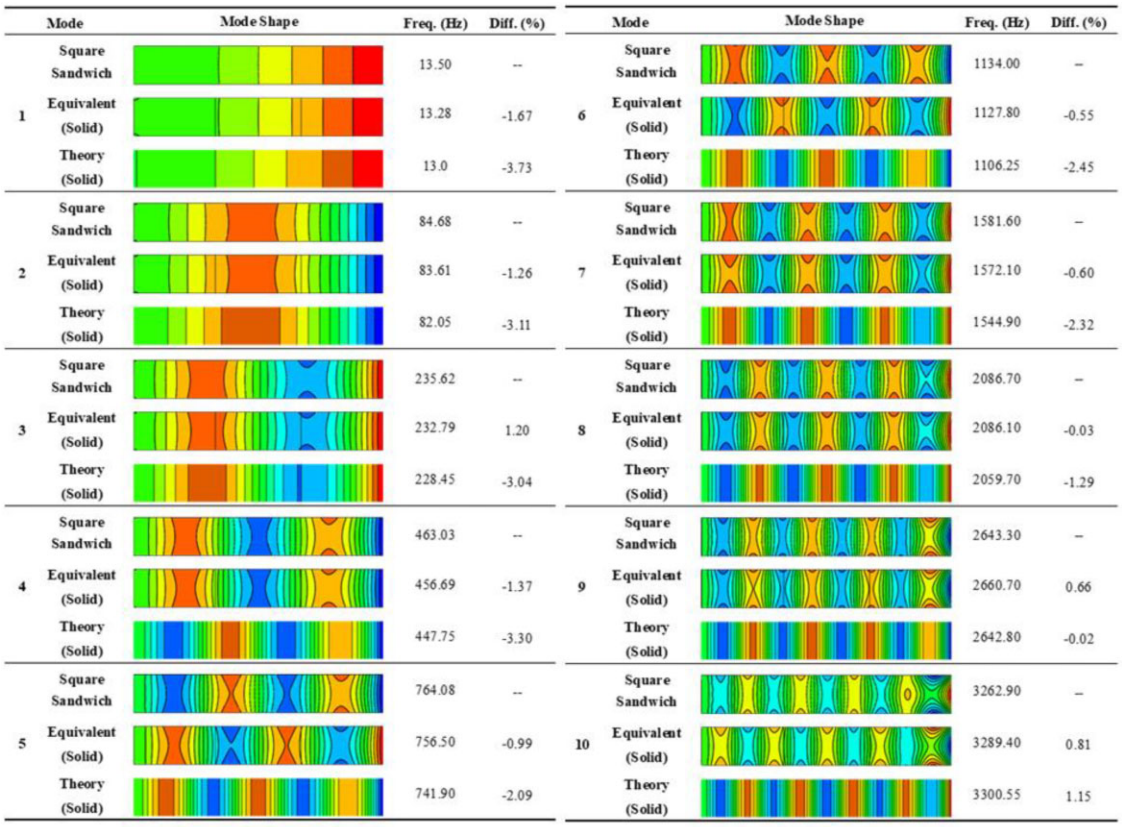

	Mode	Mode Shape	Freq. (Hz)	Diff. (%)
1	Square Sandwich		13.50	--
	Equivalent (Solid)		13.28	-1.67
	Theory (Solid)		13.0	-3.73
2	Square Sandwich		84.68	--
	Equivalent (Solid)		83.61	-1.26
	Theory (Solid)		82.05	-3.11
3	Square Sandwich		235.62	--
	Equivalent (Solid)		232.79	1.20
	Theory (Solid)		228.45	-3.04
4	Square Sandwich		463.03	--
	Equivalent (Solid)		456.69	-1.37
	Theory (Solid)		447.75	-3.30
5	Square Sandwich		764.08	--
	Equivalent (Solid)		756.50	-0.99
	Theory (Solid)		741.90	-2.09

	Mode	Mode Shape	Freq. (Hz)	Diff. (%)
6	Square Sandwich		1134.00	--
	Equivalent (Solid)		1127.80	-0.55
	Theory (Solid)		1106.25	-2.45
7	Square Sandwich		1581.60	--
	Equivalent (Solid)		1572.10	-0.60
	Theory (Solid)		1544.90	-2.32
8	Square Sandwich		2086.70	--
	Equivalent (Solid)		2086.10	-0.03
	Theory (Solid)		2059.70	-1.29
9	Square Sandwich		2643.30	--
	Equivalent (Solid)		2660.70	0.66
	Theory (Solid)		2642.80	-0.02
10	Square Sandwich		3262.90	--
	Equivalent (Solid)		3289.40	0.81
	Theory (Solid)		3300.55	1.15

Figure 26 Comparison of theoretical and numerical mode shapes of composite sandwich beams with 3 blocks filled without metal mixture.

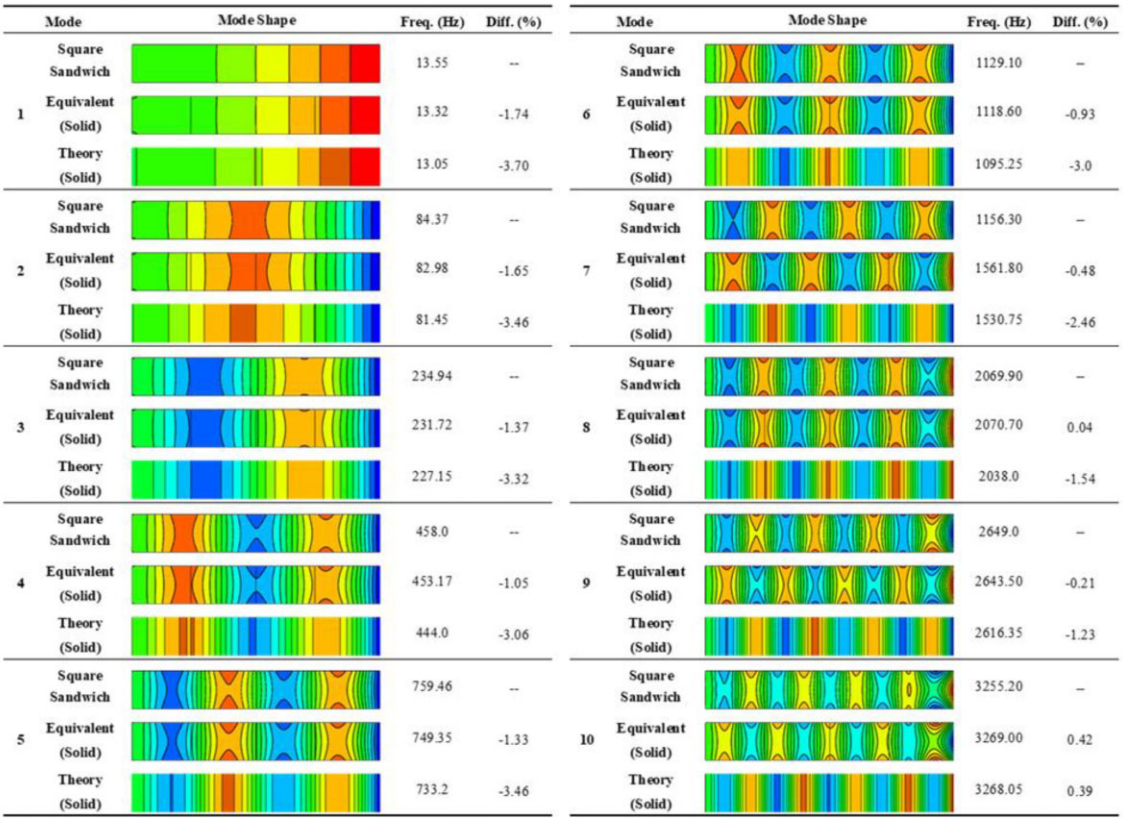

Figure 27 Comparison of theoretical and numerical mode shapes of composite sandwich beams with 4 blocks filled without metal mixture.

Table 9 Numerical natural frequencies of two composite sandwich beams filled without and with metal mixture using detailed simulations.

	Three blocks (Hz)			Four blocks (Hz)		
Mode	**Hollow**	**Filled**	**Diff. (%)**	**Hollow**	**Filled**	**Diff. (%)**
1	13.50	11.67	13.56	13.55	11.37	16.09
2	84.68	72.01	14.97	84.37	71.04	15.80
3	235.62	202.48	14.07	234.94	198.26	15.61
4	463.03	398.40	13.96	458.00	387.48	15.40
5	764.08	654.08	14.40	759.46	644.85	15.09
6	1134.00	973.10	14.19	1129.10	958.23	15.13
7	1581.60	1359.20	14.06	1569.30	1329.20	15.30
8	2086.70	1788.30	14.30	2069.90	1752.40	15.34
9	2643.30	2266.90	14.24	2649.00	2247.80	15.15
10	3262.90	2803.10	14.09	3255.20	2758.50	15.26

Table 10 Numerical natural frequencies of two composite sandwich beams filled without and with metal mixture using equivalent simulations.

	Three blocks (Hz)			Four blocks (Hz)		
Mode	**Hollow**	**Filled**	**Diff. (%)**	**Hollow**	**Filled**	**Diff. (%)**
1	13.28	11.48	13.55	13.32	11.17	16.09
2	83.61	71.13	14.93	82.98	69.89	15.78
3	232.79	200.29	13.96	231.72	195.64	15.57
4	456.69	392.99	13.95	453.17	383.85	15.30
5	756.50	647.80	14.37	749.35	636.00	15.13
6	1127.80	969.08	14.07	1118.60	949.62	15.11
7	1572.10	1351.70	14.02	1561.80	1323.40	15.26
8	2086.10	1788.50	14.27	2070.70	1754.90	15.25
9	2660.70	2285.60	14.10	2643.50	2243.00	15.15
10	3289.40	2828.70	14.01	3269.00	2772.40	15.19

Table 11 Experimental natural frequencies of two composite sandwich beams filled without and with metal mixture.

	Three blocks (Hz)			Four blocks (Hz)		
Mode	**Hollow**	**Filled**	**Diff. (%)**	**Hollow**	**Filled**	**Diff. (%)**
1	13.49	11.66	13.57	13.54	11.36	16.10
2	84.65	72.02	14.92	84.32	71.03	15.76
3	237	205	13.50	233	204	12.45
4	462	402	12.99	459	388	15.47
5	766	662	13.58	760	651	14.34
6	1035	975	5.80	1018	960	5.70
7	1583	1345	15.03	1567	1360	13.21
8	2085	1795	13.91	2070	1750	15.46
9	2645	2270	14.18	2648	2240	15.41
10	3260	2800	14.11	3260	2760	15.34

Table 12 Comparison of experimental and theoretical natural frequencies of two composite sandwich beams filled with metal mixture.

	Three blocks (Hz)			Four blocks (Hz)		
Mode	**Experiment**	**Theory**	**Diff. (%)**	**Experiment**	**Theory**	**Diff. (%)**
1	11.66	11.25	3.64	11.36	10.93	3.93
2	72.02	69.8	3.18	71.03	68.56	3.60
3	205	196.8	4.17	204	191.9	6.31
4	402	385.3	4.33	388	376.12	3.16
5	662	635.25	4.21	651	622.32	4.61
6	975	950.65	2.56	960	929.62	3.27
7	1345	1328.25	1.26	1360	1297.33	4.83
8	1795	1765.65	1.66	1750	1727.21	1.32
9	2270	2270.1	−0.004	2240	2220.29	0.89
10	2800	2836.85	−1.30	2760	2773.41	−0.48

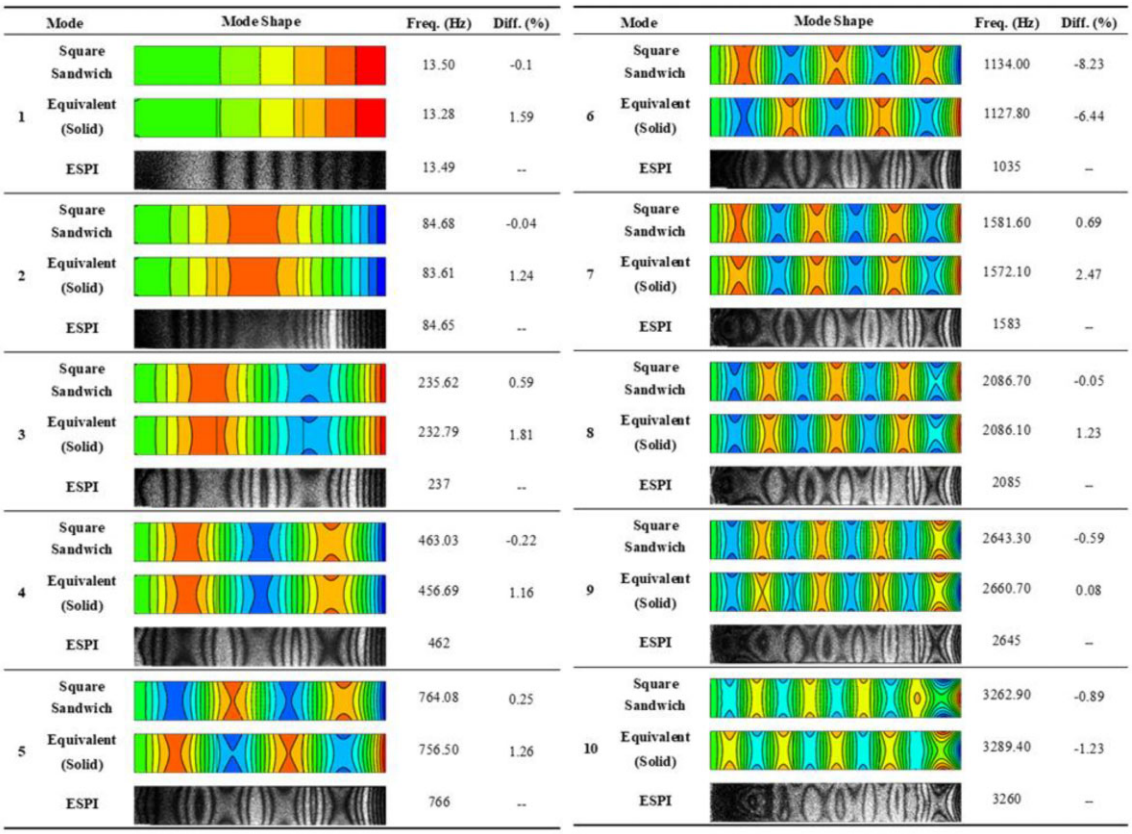

Figure 28 Comparison of experimental and numerical mode shapes of composite sandwich beams with 3 blocks filled without metal mixture.

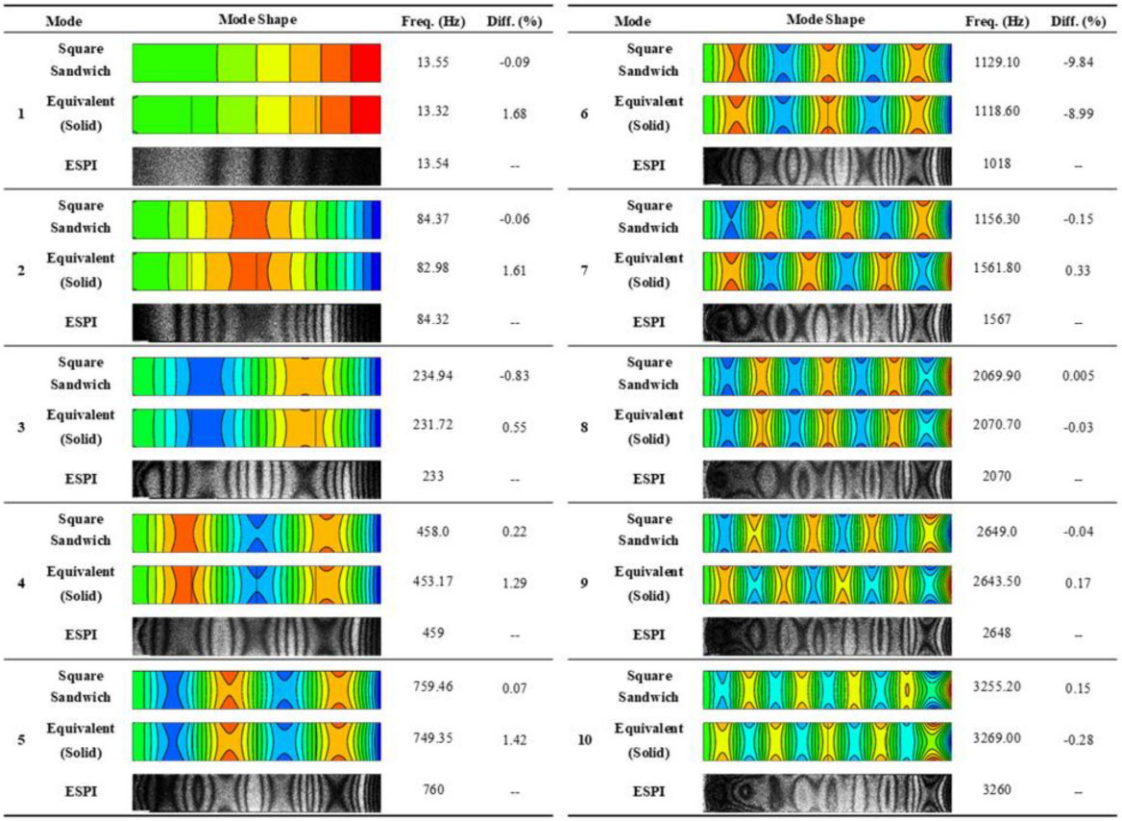

Figure 29 Comparison of experimental and numerical mode shapes of composite sandwich beams with 4 blocks filled without metal mixture.

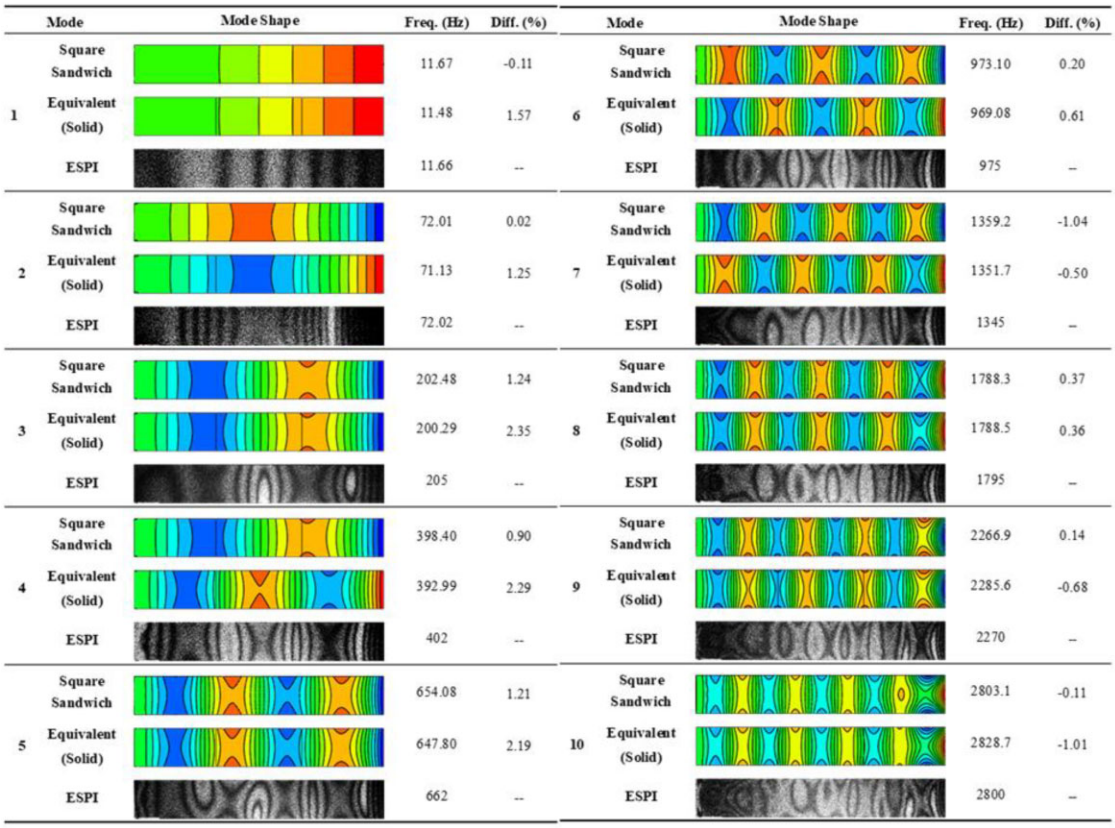

Figure 30 Comparison of experimental and numerical mode shapes of composite sandwich beams with 3 blocks filled with metal mixture.

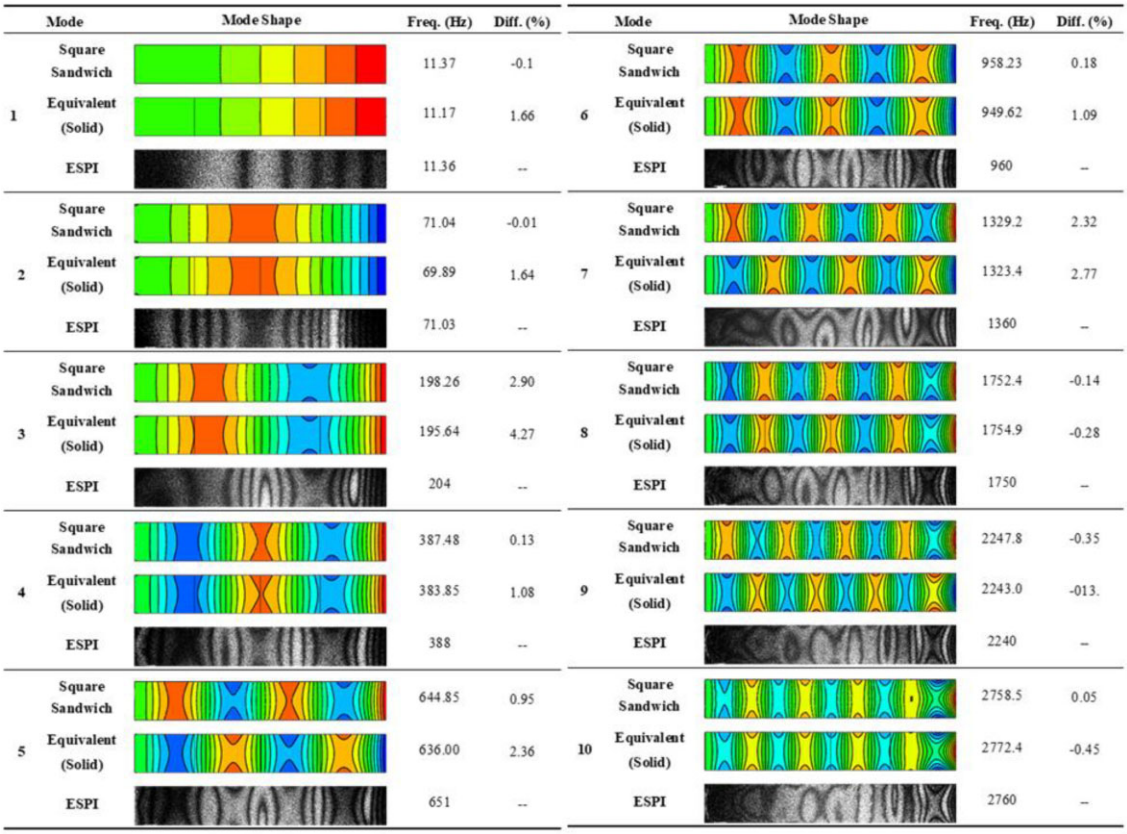

Figure 31 Comparison of experimental and numerical mode shapes of composite sandwich beams with 4 blocks filled with metal mixture.

mixture. Unlike the third mode of the 4 types of sandwich beams, the differences between numerical and experimental results of the composite beams are small. The natural frequencies of the torsion modes of the composite beams are far away from those of the third bending modes. The maximum difference between "Square Sandwich" and experimental results is −8.73% for 3-blocks sandwich beam and −9.84% for 4-blocks sandwich beam. The maximum differences occur for the sixth mode for both sandwich beams. It may be caused by a machining error. Figure 30 gives the comparison of experimental and numerical mode shapes of composite sandwich beams with 3 blocks filled with metal mixture. Figure 31 also shows the comparison of experimental and numerical mode shapes of composite sandwich beams with 4 blocks filled with metal mixture. The maximum difference between "Square Sandwich" and experimental results are 1.24% for 3-blocks sandwich beam and 2.90% for 4-blocks sandwich beam. The maximum differences occur for the third mode for both sandwich beams. Unlike the composite beams filled without metal mixture, the differences of the sixth modes between numerical and experimental results are reasonable.

5. CONCLUSIONS

In this paper, the vibration characteristics of sandwich beams with square grid cores are investigated theoretically, numerically and experimentally. The Euler–Bernoulli beam theory and equivalent parameters have proved to be accurate to predict the natural frequencies of sandwich beams with square grid cores. Two simulation methods: equivalent simulation and detailed simulation are presented. The theoretical and numerical natural frequencies and mode shapes of 3D printed sandwich beams are validated using the results measured using the AF-ESPI. It is found that filling metal mixture into the cores only changes the equivalent density. The equivalent stiffness is almost the same. The equivalent theory and simulation methods are reasonable to simulate the vibration of sandwich beams. Thus, it is possible to control the vibration characteristics of sandwich beams by filling metal mixture into the cores with almost constant stiffness. Then, the composite sandwich beams with different square grid cores are studied theoretically, numerically and experimentally. The results obtained from different methods are in good agreement with each other. The study offers a method to control the structural vibration characteristics of sandwich beams by changing the design of the square cores and filling the cores with metal mixture. In future works, the effect of the metal mixture on the damping properties of the sandwich beams will be investigated.

ACKNOWLEDGMENTS

The author, Yi-Chuang Wu, would like to express his gratitude to Prof. Chien-Ching Ma for the long relationship as a constant guidance as a mentor in the past 19 years. Looking back on the past years, Prof. Chien-Ching Ma's rigorous research attitude and kind demeanor have profoundly influenced me. Here, I extend my heartfelt gratitude and remembrance for his mentorship.

The author, Ming Ji, would like to express his heartfelt gratitude to Prof. Chien-Ching Ma for guidance in the past 12 years. Looking back, I'm truly appreciative of the invaluable knowledge and wisdom Prof. Ma has shared with me, both in terms of academic development and personal growth.

The authors would like to dedicate this paper to the memory of Prof. Chien-Ching Ma. The authors gratefully acknowledge the financial support for this study by the Ministry of Science and Technology (Republic of China) under Grants NSTC 113-2221-E-011-161.

AUTHOR CONTRIBUTIONS

Yi-Chuang Wu (Investigation, Methodology, Validation, Visualization, Writing—original draft, Project administration, Funding acquisition, Supervision), Yun-Jhen Lai (Investigation, Data curation, Software, Validation, Visualization), Jhen-Hao Syu (Investigation, Data curation, Software, Validation, Visualization), Ming Ji (Conceptualization, Investigation, Methodology, Validation, Visualization, Writing—original draft, Writing—review & editing, Supervision)

REFERENCES

1. De Souza Eloy F, Gomes GF, Ancelotti AC, Da Cunha SS, Bombard AJF, Junqueira DM. A numerical-experimental dynamic analysis of composite sandwich beam with magnetorheological elastomer honeycomb core. *Composite Structures* 2019;**209**:242–257.
2. Faria LER, Gomes GF, Gomes De Sousa SR, Bombard AJF, Ancelotti AC, Jr. Dynamic experimental behavior of sandwich beams with honeycomb core filled with magnetic rheological gel: a statistical approach. *Smart Materials and Structures* 2020;**29**(11):115044.
3. Chikh N, Nour A, Aguib S, Tawfiq I. Dynamic analysis of the non-linear behavior of a composite sandwich beam with a magnetorheological elastomer core. *Acta Mechanica Solida Sinica* 2016;**29**(3):271–283.
4. Gibson LJ, Ashby MF. *Cellular Solids: Structure and Properties*. Cambridge, UK: Cambridge University Press, 1999.
5. Wang Y-J, Zhang Z-J, Xue X-M, Zhang L. Free vibration analysis of composite sandwich panels with hierarchical honeycomb sandwich core. *Thin-Walled Structures* 2019;**145**:106425.
6. Gu JT, Sheng MP, Han F. Design square grid sandwich plate based on equivalent theory. *Applied Mechanics and Materials* 2013;**248**:365–369.
7. Steenackers G, Peeters J, Ribbens B, Vuye C. Development of an equivalent composite honeycomb model: a finite element study. *Applied Composite Materials* 2016;**23**(6):1177–1194.
8. Wang AJ, McDowell DL. In-plane stiffness and yield strength of periodic metal honeycombs. *Journal of Engineering Materials and Technology* 2004;**126**(2):137–156.
9. Lu C, Qi M, Islam S, Chen P, Gao S, Xu Y, Yang X. Mechanical performance of 3D-printing plastic honeycomb sandwich structure. *International Journal of Precision Engineering and Manufacturing-Green Technology* 2018;**5**(1):47–54.
10. Yao T, Deng Z, Zhang K, Li S. A method to predict the ultimate tensile strength of 3D printing polylactic acid (PLA) materials with different printing orientations. *Composites Part B: Engineering* 2019;**163**:393–402.
11. Fernandez-Vicente M, Calle W, Ferrandiz S, Conejero A. Effect of infill parameters on tensile mechanical behavior in desktop 3D printing. *3D Printing and Additive Manufacturing* 2016;**3**(3):183–192.
12. Dai G, Zhang W. Cell size effects for vibration analysis and design of sandwich beams. *Acta Mechanica Sinica* 2009;**25**(3):353–365.
13. Butters JN, Leendertz JA. Speckle pattern and holographic techniques in engineering metrology. *Optics & Laser Technology* 1971;**3**(1):26–30.
14. Høgmoen K, Løkberg OJ. Detection and measurement of small vibrations using electronic speckle pattern interferometry. *Applied Optics* 1977;**16**(7):1869–1875.
15. Moore AJ, Tyrer JR. Two-dimensional strain measurement with ESPI. *Optics and Lasers in Engineering* 1996;**24**(5-6):381–402.
16. Wang WC, Hwang CH, Lin SY. Vibration measurement by the time-averaged electronic speckle pattern interferometry methods. *Applied Optics* 1996;**35**(22):4502–4509.
17. Huang CH, Ma CC. Experimental measurement of mode shapes and frequencies for vibration of plates by optical interferometry method. *Journal of Vibration and Acoustics* 2001;**123**(2):276–280.
18. Ma CC, Hsieh DM. Full-field experimental investigations on resonant vibration of cracked rectangular cantilever plates. *AIAA Journal* 2001;**39**(12):2419–2422.
19. Wu YC, Ma CC, Liou HC. Theoretical analysis and experimental measurement of coupling dynamic characteristics for transversely isotropic rectangular plate based on modified FSDT assumption. *Acta Mechanica* 2020;**231**(10):4275–4321.
20. Dai GZ, Wu YC, Ma CC. A novel solution for dynamic behaviors of multi-span bridge plates. *International Journal of Mechanical Sciences* 2025;**285**:109798.
21. Liao C-Y, Wu Y-C, Chang C-Y, Ma C-C. Theoretical analysis based on fundamental functions of thin plate and experimental measurement for vibration characteristics of a plate coupled with liquid. *Journal of Sound and Vibration* 2017;**394**:545–574.
22. Liao C-Y, Chen G-W, Hsu H-W, Ma C-C. Theoretical analysis of vibration characteristics of rectangular thin plate fully immersed in fluid with finite dimension. *International Journal of Mechanical Sciences* 2021;**189**:105979.
23. Chen G-W, Liao C-Y, Lin Y-Z, Lee K-T, Ma C-C. Analytical solution for the vibration characteristics of a partially immersed plate with experimental investigation on wet mode shapes. *Applied Mathematical Modelling* 2022;**111**:1–43.
24. Liao CY, Chen GW, Ma CC. Transient behavior of a plate partially immersed in the fluid subjected to impact loadings: theoretical analysis and experimental measurements. *Thin-Walled Structures* 2024;**202**:112134.
25. Ma CC, Lin CC. Experimental investigation of vibrating laminated composite plates by optical interferometry method. *AIAA Journal* 2001;**39**(3):491–497.

26. Ma CC, Huang CH. The investigation of three-dimensional vibration for piezoelectric rectangular parallelepipeds using the AF-ESPI method. *IEEE Transactions on Ultrasonics, Ferroelectrics, and Frequency Control* 2001;**48**(1):142–153.
27. Huang CH, Ma CC. Experimental and numerical investigations of resonant vibration characteristics for piezoceramic plates. *The Journal of the Acoustical Society of America* 2001;**109**(6):2780–2788.
28. Ma CC, Huang CH. Experimental full field investigations of resonant vibrations for piezoceramic plates by an optical interferometry method. *Experimental Mechanics* 2002;**42**(2):140–146.
29. Chi-Hung Huang, Yu-Chih Lin, Chien Ching Ma. Theoretical analysis and experimental measurement for resonant vibration of piezoceramic circular plates. *IEEE Transactions on Ultrasonics, Ferroelectrics and Frequency Control* 2004;**51**(1):12–24.
30. Chi-Hung Huang, Chien-Ching Ma, Yu-Chih Lin. Theoretical, numerical, and experimental investigation on resonant vibrations of piezoceramic annular disks. *IEEE Transactions on Ultrasonics, Ferroelectrics and Frequency Control* 2005;**52**(8):1204–1216.
31. Ma CC, Lin HY. Experimental measurements on transverse vibration characteristics of piezoceramic rectangular plates by optical methods. *Journal of Sound and Vibration* 2005;**286**(3):587–600.
32. Chang CY, Ma CC. Mode-shape measurement of piezoelectric plate using temporal speckle pattern interferometry and temporal standard deviation. *Optics Letters* 2011;**36**(21):4281–4283.
33. Ma CC, Chang CY. Improving image-quality of interference fringes of out-of-plane vibration using temporal speckle pattern interferometry and standard deviation for piezoelectric plates. *IEEE Transactions on Ultrasonics, Ferroelectrics, and Frequency Control* 2013;**60**(7):1412–1423.
34. Huang YH, Ma CC, Li ZZ. Investigations on vibration characteristics of two-layered piezoceramic disks. *International Journal of Solids and Structures* 2014;**51**(1):227–251.
35. Wu YC, Huang YH, Ma CC. Theoretical analysis and experimental measurement of flexural vibration and dynamic characteristics for piezoelectric rectangular plate. *Sensors and Actuators A: Physical* 2017;**264**:308–332.
36. Huang CH, Ma CC. Vibration characteristics for piezoelectric cylinders using amplitude-fluctuation electronic speckle pattern interferometry. *AIAA Journal* 1998;**36**(12):2262–2268.
37. Yu-Hsi Huang, Chien-Ching Ma. Experimental measurements and finite element analysis of the coupled vibrational characteristics of piezoelectric shells. *IEEE Transactions on Ultrasonics, Ferroelectrics and Frequency Control* 2012;**59**(4):785–798.
38. Ji M, Tai KH, Wu YC. Investigation into vibration excitation and mode selection of thin rectangular plates with multiple bolts and stand-off supports. *International Journal of Structural Stability and Dynamics* 2024;**24**(19):2450219.
39. Wu YC. Accurate dynamic electromechanical solution for rectangular piezoelectric plate based on modified FSDT. *International Journal of Structural Stability and Dynamics* 2023;**23**(19):2350181.
40. Ji M, Zhong JJ, Wu YC. Higher-order shear deformation theory for accurate prediction of vibration behavior of thick piezoelectric disks and design of efficient surface electrodes. *International Journal of Solids and Structures* 2024;**290**:112669.
41. Ji M, Zhong J-J, Huang Y-H, Wu Y-C. Theoretical, numerical and experimental investigation into vibration characteristics for composite structures of an annular membrane internally connected with a piezoceramic disk. *Journal of Mechanics* 2023;**39**:451–470.

Received: 9 December 2024; **Revised:** 12 February 2025; **Accepted:** 17 March 2025